Neutron-proton scattering with lattice chiral effective field theory at next-to-next-to-next-to-leading order

Ning Li,[1,*] Serdar Elhatisari,[2,3] Evgeny Epelbaum,[4] Dean Lee,[1,5] Bing-Nan Lu,[1] and Ulf-G. Meißner[2,6,7]

[1]*Facility for Rare Isotope Beams and Department of Physics and Astronomy, Michigan State University, Michigan 48824, USA*
[2]*Helmholtz-Institut für Strahlen- und Kernphysik and Bethe Center for Theoretical Physics, Universität Bonn, D-53115 Bonn, Germany*
[3]*Department of Physics, Karamanoglu Mehmetbey University, Karaman 70100, Turkey*
[4]*Institut für Theoretische Physik II, Ruhr-Universität Bochum, D-44870 Bochum, Germany*
[5]*Department of Physics, North Carolina State University, Raleigh, North Carolina 27695, USA*
[6]*Institute for Advanced Simulation, Institut für Kernphysik, and Jülich Center for Hadron Physics, Forschungszentrum Jülich, D-52425 Jülich, Germany*
[7]*JARA—High Performance Computing, Forschungszentrum Jülich, D-52425 Jülich, Germany*

(Received 30 June 2018; published 16 October 2018)

We present a new lattice formulation of chiral effective field theory interactions with a simpler decomposition into spin channels. With these interactions the process of fitting to the empirical scattering phase shifts is simplified, and the resulting lattice phase shifts are more accurate than in previous studies. We present results for the neutron-proton system up to next-to-next-to-next-to-leading order for lattice spacings of 1.97, 1.64, 1.32, and 0.99 fm. Our results provide a pathway to *ab initio* lattice calculations of nuclear structure, reactions, and thermodynamics with accurate and systematic control over the chiral nucleon-nucleon force.

DOI: 10.1103/PhysRevC.98.044002

I. INTRODUCTION

Chiral effective field theory (EFT) organizes the interactions of nucleons in powers of momenta and factors of the pion mass near the chiral limit where the light quarks are massless. We label terms that carry a total of n powers of nucleon momenta or factors of the pion masses as order Q^n. The most important interactions at low energy are at order Q^0, or leading order (LO). Next-to-leading-order (NLO) interactions correspond to order Q^2, next-to-next-to-leading-order (N^2LO) terms to Q^3, and next-to-next-to-next-to-leading-order (N^3LO) to Q^4. See Ref. [1] for a review of chiral EFT. Nuclear lattice simulations using chiral EFT have been used in recent years to describe the structure and scattering of atomic nuclei [2–7]. However, the treatment of nuclear forces at higher orders in the chiral EFT expansion is more difficult on the lattice due to the breaking of rotational invariance produced by nonzero lattice spacing [8,9]. Fitting the unknown coefficients of the short-range lattice interactions to empirical phase shifts can introduce significant uncertainties.

In this paper we solve these problems by introducing a new set of short-range chiral EFT interactions on the lattice with a simpler decomposition into spin channels. The angular dependence of the relative separation between the two nucleons is prescribed by spherical harmonics, and the dependence on the nucleon spins is given by the spin-orbit Clebsch-Gordan coefficients. The full details of this process are presented in this paper. We start with some definitions of the lattice operator notations used. Next we discuss the lattice Hamiltonian used in our lattice transfer matrix formalism. The short-range interactions are presented first, and we then proceed to the long-range interactions. We then compare our neutron-proton scattering results at lattice spacings of 1.97, 1.64, 1.32, and 0.99 fm with the empirical phase shifts. After this we compute some observable properties of the deuteron, discuss theoretical uncertainties, and present a summary and outlook. Certain interactions such as the Coulomb interaction and some isospin-breaking interactions are not directly relevant to the neutron-proton analysis that we consider here. However, we include these interactions in this work for completeness and future reference.

II. LATTICE OPERATOR DEFINITIONS

Let us define $a_{i,j}(\mathbf{n})$ and $a^\dagger_{i,j}(\mathbf{n})$, the lattice annihilation and creation operators at lattice site $\mathbf{n}$ with spin $i = 0, 1$ (up, down) and isospin $j = 0, 1$ (proton, neutron). The operators $a^{s_{\rm NL}}_{i,j}(\mathbf{n})$ and $a^{s_{\rm NL}\dagger}_{i,j}(\mathbf{n})$ are defined via nonlocal smearing with the real parameter $s_{\rm NL}$,

$$a^{s_{\rm NL}}_{i,j}(\mathbf{n}) = a_{i,j}(\mathbf{n}) + s_{\rm NL}\sum_{|\mathbf{n}'|=1} a_{i,j}(\mathbf{n}+\mathbf{n}'). \tag{1}$$

$$a^{s_{\rm NL}\dagger}_{i,j}(\mathbf{n}) = a^\dagger_{i,j}(\mathbf{n}) + s_{\rm NL}\sum_{|\mathbf{n}'|=1} a^\dagger_{i,j}(\mathbf{n}+\mathbf{n}'). \tag{2}$$

Next we define the pair annihilation operators $[a(\mathbf{n})a(\mathbf{n}')]^{s_{\rm NL}}_{S,S_z,I,I_z}$, where

$$[a(\mathbf{n})a(\mathbf{n}')]^{s_{\rm NL}}_{S,S_z,I,I_z} = \sum_{i,j,i',j'} a^{s_{\rm NL}}_{i,j}(\mathbf{n}) M_{ii'}(S,S_z) M_{jj'}(I,I_z) a^{s_{\rm NL}}_{i',j'}(\mathbf{n}') \tag{3}$$

*lini@frib.msu.edu

 ©2018 American Physical Society

with

$$M_{ii'}(0,0) = \frac{1}{\sqrt{2}}[\delta_{i,0}\delta_{i',1} - \delta_{i,1}\delta_{i',0}], \tag{4}$$

$$M_{ii'}(1,1) = \delta_{i,0}\delta_{i',0}, \tag{5}$$

$$M_{ii'}(1,0) = \frac{1}{\sqrt{2}}[\delta_{i,0}\delta_{i',1} + \delta_{i,1}\delta_{i',0}], \tag{6}$$

$$M_{ii'}(1,-1) = \delta_{i,1}\delta_{i',1}. \tag{7}$$

We define the lattice finite difference operation ∇_l on a general lattice function $f(\mathbf{n})$ as

$$\nabla_l f(\mathbf{n}) = \tfrac{1}{2} f(\mathbf{n}+\hat{\mathbf{l}}) - \tfrac{1}{2} f(\mathbf{n}-\hat{\mathbf{l}}), \tag{8}$$

where $\hat{\mathbf{l}}$ is the spatial lattice unit vector in the l direction. It is also convenient to define the lattice finite difference operation $\nabla_{1/2,l}$ defined on points halfway between lattice sites:

$$\nabla_{1/2,l} f(\mathbf{n}) = f\left(\mathbf{n}+\tfrac{1}{2}\hat{\mathbf{l}}\right) - f\left(\mathbf{n}-\tfrac{1}{2}\hat{\mathbf{l}}\right). \tag{9}$$

We use this operation only to define the Laplacian operator,

$$\nabla^2_{1/2} = \sum_l \nabla^2_{1/2,l}. \tag{10}$$

Let us define the solid harmonics

$$R_{L,L_z}(\mathbf{r}) = \sqrt{\frac{4\pi}{2L+1}} r^L Y_{L,L_z}(\theta,\phi) \tag{11}$$

and their complex conjugates

$$R^*_{L,L_z}(\mathbf{r}) = \sqrt{\frac{4\pi}{2L+1}} r^L Y^*_{L,L_z}(\theta,\phi). \tag{12}$$

Using the pair annihilation operators, lattice finite differences, and solid harmonics, we define the operator

$$P^{2M,s_{\rm NL}}_{S,S_z,L,L_z,I,I_z}(\mathbf{n}) = \left[a(\mathbf{n})\nabla^{2M}_{1/2} R^*_{L,L_z}(\nabla) a(\mathbf{n})\right]^{s_{\rm NL}}_{S,S_z,I,I_z}, \tag{13}$$

where $\nabla^{2M}_{1/2}$ and ∇ act on the second annihilation operator. More explicitly stated, this means that we act on the $\mathbf{n}'$ in Eq. (3) and then set $\mathbf{n}'$ to equal $\mathbf{n}$. The even integer $2M$ gives us higher powers of the finite differences. Writing the Clebsch-Gordan coefficients as $\langle SS_z, LL_z | JJ_z\rangle$, we define

$$O^{2M,s_{\rm NL}}_{S,L,J,J_z,I,I_z}(\mathbf{n}) = \sum_{S_z,L_z} \langle SS_z, LL_z | JJ_z\rangle P^{2M,s_{\rm NL}}_{S,S_z,L,L_z,I,I_z}(\mathbf{n}). \tag{14}$$

We also define pointlike density operators that depend on spin and isospin. For spin indices $S = 1, 2, 3,$ and isospin indices $I = 1, 2, 3$, we define

$$\rho(\mathbf{n}) = \sum_{i,j} a^\dagger_{i,j}(\mathbf{n}) a_{i,j}(\mathbf{n}), \tag{15}$$

$$\rho_S(\mathbf{n}) = \sum_{i,i',j} a^\dagger_{i,j}(\mathbf{n}) [\sigma_S]_{ii'} a_{i',j}(\mathbf{n}), \tag{16}$$

$$\rho_I(\mathbf{n}) = \sum_{i,j,j'} a^\dagger_{i,j}(\mathbf{n}) [\tau_I]_{jj'} a_{i,j'}(\mathbf{n}), \tag{17}$$

$$\rho_{S,I}(\mathbf{n}) = \sum_{i,i',j,j'} a^\dagger_{i,j}(\mathbf{n}) [\sigma_S]_{ii'} \otimes [\tau_I]_{jj'} a_{i',j'}(\mathbf{n}), \tag{18}$$

where σ_S are Pauli matrices in spin space and τ_I are Pauli matrices in isospin space.

III. LATTICE HAMILTONIAN AND TRANSFER MATRIX FORMALISM

Let a be the spatial lattice spacing and a_t be the temporal lattice spacing. We work in lattice units (l.u.), where all quantities are multiplied by the powers of the spatial spacing to form a dimensionless combination. The normal-ordered transfer matrix is

$$M =: \exp[-H\alpha_t] :, \tag{19}$$

where the :: symbols denote normal ordering where the annihilation operators are on the right and creation operators are on the left. $\alpha_t = a_t/a$ is the ratio between the temporal lattice spacing and the spacial lattice spacing. For the temporal lattice spacing, we take $a_t = 1.32$ fm for $a = 1.97$ fm. We rescale a_t for other lattice spacings so that a^2/a_t is fixed. We partition the lattice Hamiltonian H into a free Hamiltonian, short-range interactions, and long-range interactions,

$$H = H_{\rm free} + V^{\rm short}_{\rm 2N} + V^{\rm long}_{\rm 2N}. \tag{20}$$

For the free Hamiltonian we use an $O(a^4)$-improved action of the form [10]

$$\begin{aligned} H_{\rm free} = {} & \frac{49}{12m}\sum_{\mathbf{n}} a^\dagger(\mathbf{n})a(\mathbf{n}) - \frac{3}{4m}\sum_{\mathbf{n},i}\sum_{\langle\mathbf{n}'\,\mathbf{n}\rangle_i} a^\dagger(\mathbf{n}')a(\mathbf{n}) \\ & + \frac{3}{40m}\sum_{\mathbf{n},i}\sum_{\langle\langle\mathbf{n}'\,\mathbf{n}\rangle\rangle_i} a^\dagger(\mathbf{n}')a(\mathbf{n}) \\ & - \frac{1}{180m}\sum_{\mathbf{n},i}\sum_{\langle\langle\langle\mathbf{n}'\,\mathbf{n}\rangle\rangle\rangle_i} a^\dagger(\mathbf{n}')a(\mathbf{n}). \end{aligned} \tag{21}$$

IV. SHORT-RANGE INTERACTIONS

A. Order Q^0

At order Q^0 we have two short-range interaction operators, namely, the S-wave spin singlet, which we call $V_{0,^1S_0}(\mathbf{n})$,

$$\sum_{I_z=-1,0,1} \left[O^{0,s_{\rm NL}}_{0,0,0,0,1,I_z}(\mathbf{n})\right]^\dagger O^{0,s_{\rm NL}}_{0,0,0,0,1,I_z}(\mathbf{n}), \tag{22}$$

and the S-wave spin triplet $V_{0,^3S_1}(\mathbf{n})$,

$$\sum_{J_z=-1,0,1} \left[O^{0,s_{\rm NL}}_{1,0,1,J_z,0,0}(\mathbf{n})\right]^\dagger O^{0,s_{\rm NL}}_{1,0,1,J_z,0,0}(\mathbf{n}). \tag{23}$$

We note that since we work with interactions that act with a specified parity and specified total intrinsic spin S, when we act on two-nucleon states with a total momentum equal to 0, the total isospin I is completely constrained by the requirement of overall antisymmetry of the two nucleons. However, we still specify the correct total isospin I explicitly in order to remove lattice artifacts that might otherwise appear in cases when the total momentum is not 0.

Wigner's SU(4) symmetry [11] is an approximate symmetry of the low-energy nucleon-nucleon interactions, where the nucleonic spin and isospin degrees of freedom can be

rotated as four components of an SU(4) multiplet. As in previous work [7], we treat the SU(4) part of the short-range interactions separately. This choice allows us to control the strength of the local part of the SU(4) interaction, which has been shown to be important for the binding of nucleons in nuclei [6]. So at leading order we also include an SU(4)-invariant short-range operator V_0 with the form

$$V_0 = \frac{C_0}{2} : \sum_{\mathbf{n}',\mathbf{n},\mathbf{n}''} \sum_{i',j'} a^{s_{\rm NL}\dagger}_{i',j'}(\mathbf{n}') a^{s_{\rm NL}}_{i',j'}(\mathbf{n}') f_{s_{\rm L}}(\mathbf{n}'-\mathbf{n}) f_{s_{\rm L}}(\mathbf{n}-\mathbf{n}'') \times \sum_{i'',j''} a^{s_{\rm NL}\dagger}_{i'',j''}(\mathbf{n}'') a^{s_{\rm NL}}_{i'',j''}(\mathbf{n}'') :, \quad (24)$$

where $f_{s_{\rm L}}$ is defined as

$$\begin{aligned} f_{s_{\rm L}}(\mathbf{n}) &= 1 \quad \text{for} \quad |\mathbf{n}| = 0, \\ &= s_L \quad \text{for} \quad |\mathbf{n}| = 1, \\ &= 0 \quad \text{otherwise}. \end{aligned} \quad (25)$$

We repeat again that, in terms of counting powers of momentum, this SU(4) interaction is equivalent to the SU(4)-invariant interaction we get by adding together $V_{0,{}^1S_0}(\mathbf{n})$ and $V_{0,{}^3S_1}(\mathbf{n})$. However, the separate treatment of this interaction allows us to control the strength of the local part of the SU(4) interaction in systems with more than a few nucleons. For the purposes of fitting operator coefficients, we keep the coefficient C_0 fixed and tune the coefficients of $V_{0,{}^1S_0}(\mathbf{n})$ and $V_{0,{}^3S_1}(\mathbf{n})$ as needed to reproduce the scattering phase shifts and mixing angles. In this work we take the smearing parameter $s_{\rm NL}$ for the SU(4) interaction to be the same as that used in the other short-range interactions. For $a = 1.97$ fm we take $C_0 = -0.175$ l.u., $s_L = 0.070$ l.u, and $s_{\rm NL} = 0.080$ l.u. For $a = 1.64$ fm we use $C_0 = -0.100$ l.u., $s_L = 0.109$ l.u, and $s_{\rm NL} = 0.122$ l.u. For $a = 1.32$ fm, we use $C_0 = -0.045$ l.u., $s_L = 0.170$ l.u, and $s_{\rm NL} = 0.186$ l.u. For $a = 0.99$ fm, we use $C_0 = -0.015$ l.u., $s_L = 0.265$ l.u, and $s_{\rm NL} = 0.283$ l.u. In future work, however, we may consider different smearing parameters for the two cases in order to accelerate the convergence of the effective field theory expansion in many-body systems.

B. Order Q^2

At order Q^2 we have the lowest radial excitations of the S-wave spin singlet, which we call $V_{2,{}^1S_0}(\mathbf{n})$,

$$\sum_{I_z=-1,0,1} \left[O^{2,s_{\rm NL}}_{0,0,0,0,1,I_z}(\mathbf{n})\right]^\dagger O^{0,s_{\rm NL}}_{0,0,0,0,1,I_z}(\mathbf{n}) + \sum_{I_z=-1,0,1} \left[O^{0,s_{\rm NL}}_{0,0,0,0,1,I_z}(\mathbf{n})\right]^\dagger O^{2,s_{\rm NL}}_{0,0,0,0,1,I_z}(\mathbf{n}), \quad (26)$$

and the S-wave spin triplet $V_{2,{}^3S_1}(\mathbf{n})$,

$$\sum_{J_z=-1,0,1} \left[O^{2,s_{\rm NL}}_{1,0,1,J_z,0,0}(\mathbf{n})\right]^\dagger O^{0,s_{\rm NL}}_{1,0,1,J_z,0,0}(\mathbf{n}) + \sum_{J_z=-1,0,1} \left[O^{0,s_{\rm NL}}_{1,0,1,J_z,0,0}(\mathbf{n})\right]^\dagger O^{2,s_{\rm NL}}_{1,0,1,J_z,0,0}(\mathbf{n}). \quad (27)$$

At order Q^2 there is the ${}^1P_1$ interaction $V_{2,{}^1P_1}(\mathbf{n})$,

$$\sum_{J_z=-1,0,1} \left[O^{0,s_{\rm NL}}_{0,1,1,J_z,0,0}(\mathbf{n})\right]^\dagger O^{0,s_{\rm NL}}_{0,1,1,J_z,0,0}(\mathbf{n}), \quad (28)$$

the ${}^3P_0$ interaction $V_{2,{}^3P_0}(\mathbf{n})$,

$$\sum_{I_z=-1,0,1} \left[O^{0,s_{\rm NL}}_{1,1,0,0,1,I_z}(\mathbf{n})\right]^\dagger O^{0,s_{\rm NL}}_{1,1,0,0,1,I_z}(\mathbf{n}), \quad (29)$$

the ${}^3P_1$ interaction $V_{2,{}^3P_1}(\mathbf{n})$,

$$\sum_{I_z=-1,0,1} \sum_{J_z=-1,0,1} \left[O^{0,s_{\rm NL}}_{1,1,1,J_z,1,I_z}(\mathbf{n})\right]^\dagger O^{0,s_{\rm NL}}_{1,1,1,J_z,1,I_z}(\mathbf{n}), \quad (30)$$

and the ${}^3P_2$ interaction $V_{2,{}^3P_2}(\mathbf{n})$,

$$\sum_{I_z=-1,0,1} \sum_{J_z=-2,\ldots,2} \left[O^{0,s_{\rm NL}}_{1,1,2,J_z,1,I_z}(\mathbf{n})\right]^\dagger O^{0,s_{\rm NL}}_{1,1,2,J_z,1,I_z}(\mathbf{n}). \quad (31)$$

At order Q^2 we also have the S-D mixing term $V_{2,SD}(\mathbf{n})$,

$$\sum_{J_z=-1,0,1} \left[O^{0,s_{\rm NL}}_{1,2,1,J_z,0,0}(\mathbf{n})\right]^\dagger O^{0,s_{\rm NL}}_{1,0,1,J_z,0,0}(\mathbf{n}) + \sum_{J_z=-1,0,1} \left[O^{0,s_{\rm NL}}_{1,0,1,J_z,0,0}(\mathbf{n})\right]^\dagger O^{0,s_{\rm NL}}_{1,2,1,J_z,0,0}(\mathbf{n}). \quad (32)$$

C. Order Q^4

At order Q^4 we have the next-to-lowest radial excitations of the S-wave spin singlet $V_{4,{}^1S_0,1}(\mathbf{n})$,

$$\sum_{I_z=-1,0,1} \left[O^{2,s_{\rm NL}}_{0,0,0,0,1,I_z}(\mathbf{n})\right]^\dagger O^{2,s_{\rm NL}}_{0,0,0,0,1,I_z}(\mathbf{n}), \quad (33)$$

and $V_{4,{}^1S_0,2}(\mathbf{n})$,

$$\sum_{I_z=-1,0,1} \left[O^{4,s_{\rm NL}}_{0,0,0,0,1,I_z}(\mathbf{n})\right]^\dagger O^{0,s_{\rm NL}}_{0,0,0,0,1,I_z}(\mathbf{n}) + \sum_{I_z=-1,0,1} \left[O^{0,s_{\rm NL}}_{0,0,0,0,1,I_z}(\mathbf{n})\right]^\dagger O^{4,s_{\rm NL}}_{0,0,0,0,1,I_z}(\mathbf{n}), \quad (34)$$

and the next-to-lowest radial excitations of the S-wave spin triplet $V_{4,{}^3S_1,1}(\mathbf{n})$,

$$\sum_{J_z=-1,0,1} \left[O^{2,s_{\rm NL}}_{1,0,1,J_z,0,0}(\mathbf{n})\right]^\dagger O^{2,s_{\rm NL}}_{1,0,1,J_z,0,0}(\mathbf{n}), \quad (35)$$

and $V_{4,{}^3S_1,2}(\mathbf{n})$,

$$\sum_{J_z=-1,0,1} \left[O^{4,s_{\rm NL}}_{1,0,1,J_z,0,0}(\mathbf{n})\right]^\dagger O^{0,s_{\rm NL}}_{1,0,1,J_z,0,0}(\mathbf{n}) + \sum_{J_z=-1,0,1} \left[O^{0,s_{\rm NL}}_{1,0,1,J_z,0,0}(\mathbf{n})\right]^\dagger O^{4,s_{\rm NL}}_{1,0,1,J_z,0,0}(\mathbf{n}). \quad (36)$$

If we apply the on-shell equivalence condition that the magnitude of the outgoing relative momentum equals the magnitude of the incoming relative momentum, then $V_{4,{}^1S_0,1}$ and $V_{4,{}^1S_0,2}$ are equivalent and also $V_{4,{}^3S_1,1}$ and $V_{4,{}^3S_1,2}$ are equivalent. In this work we make the choice of setting the coefficients of $V_{4,{}^1S_0,2}$ and $V_{4,{}^3S_1,2}$ to 0.

At order Q^4 we have the first radial excitations of the ${}^1P_1$ interaction $V_{4,{}^1P_1}(\mathbf{n})$,

$$\sum_{J_z=-1,0,1} \left[O^{2,s_{\rm NL}}_{0,1,1,J_z,0,0}(\mathbf{n})\right]^\dagger O^{0,s_{\rm NL}}_{0,1,1,J_z,0,0}(\mathbf{n}) + \sum_{J_z=-1,0,1} \left[O^{0,s_{\rm NL}}_{0,1,1,J_z,0,0}(\mathbf{n})\right]^\dagger O^{2,s_{\rm NL}}_{0,1,1,J_z,0,0}(\mathbf{n}), \tag{37}$$

the ${}^3P_0$ interaction $V_{4,{}^3P_0}(\mathbf{n})$,

$$\sum_{I_z=-1,0,1} \left[O^{2,s_{\rm NL}}_{1,1,0,0,1,I_z}(\mathbf{n})\right]^\dagger O^{0,s_{\rm NL}}_{1,1,0,0,1,I_z}(\mathbf{n}) + \sum_{I_z=-1,0,1} \left[O^{0,s_{\rm NL}}_{1,1,0,0,1,I_z}(\mathbf{n})\right]^\dagger O^{2,s_{\rm NL}}_{1,1,0,0,1,I_z}(\mathbf{n}), \tag{38}$$

the ${}^3P_1$ interaction $V_{4,{}^3P_1}(\mathbf{n})$,

$$\sum_{I_z=-1,0,1}\sum_{J_z=-1,0,1} \left[O^{2,s_{\rm NL}}_{1,1,1,J_z,1,I_z}(\mathbf{n})\right]^\dagger O^{0,s_{\rm NL}}_{1,1,1,J_z,1,I_z}(\mathbf{n}) + \sum_{I_z=-1,0,1}\sum_{J_z=-1,0,1} \left[O^{0,s_{\rm NL}}_{1,1,1,J_z,1,I_z}(\mathbf{n})\right]^\dagger O^{2,s_{\rm NL}}_{1,1,1,J_z,1,I_z}(\mathbf{n}), \tag{39}$$

and the ${}^3P_2$ interaction $V_{4,{}^3P_2}(\mathbf{n})$,

$$\sum_{I_z=-1,0,1}\sum_{J_z=-2,\ldots,2} \left[O^{2,s_{\rm NL}}_{1,1,2,J_z,1,I_z}(\mathbf{n})\right]^\dagger O^{0,s_{\rm NL}}_{1,1,2,J_z,1,I_z}(\mathbf{n}) + \sum_{I_z=-1,0,1}\sum_{J_z=-2,\ldots,2} \left[O^{0,s_{\rm NL}}_{1,1,2,J_z,1,I_z}(\mathbf{n})\right]^\dagger O^{2,s_{\rm NL}}_{1,1,2,J_z,1,I_z}(\mathbf{n}). \tag{40}$$

At order Q^4 we also have the first radial excitations of the S-D mixing term $V_{4,SD,1}(\mathbf{n})$,

$$\sum_{J_z=-1,0,1} \left[O^{2,s_{\rm NL}}_{1,2,1,J_z,0,0}(\mathbf{n})\right]^\dagger O^{0,s_{\rm NL}}_{1,0,1,J_z,0,0}(\mathbf{n}) + \sum_{J_z=-1,0,1} \left[O^{0,s_{\rm NL}}_{1,0,1,J_z,0,0}(\mathbf{n})\right]^\dagger O^{2,s_{\rm NL}}_{1,2,1,J_z,0,0}(\mathbf{n}), \tag{41}$$

and $V_{4,SD,2}(\mathbf{n})$,

$$\sum_{J_z=-1,0,1} \left[O^{0,s_{\rm NL}}_{1,2,1,J_z,0,0}(\mathbf{n})\right]^\dagger O^{2,s_{\rm NL}}_{1,0,1,J_z,0,0}(\mathbf{n}) + \sum_{J_z=-1,0,1} \left[O^{2,s_{\rm NL}}_{1,0,1,J_z,0,0}(\mathbf{n})\right]^\dagger O^{0,s_{\rm NL}}_{1,2,1,J_z,0,0}(\mathbf{n}). \tag{42}$$

If we apply the on-shell equivalence condition, then $V_{4,SD,1}$ and $V_{4,SD,2}$ are equivalent. In this work we make the choice of setting the coefficient of $V_{4,SD,1}$ to 0.

At order Q^4 we have the ${}^1D_2$ interaction $V_{4,{}^1D_2}(\mathbf{n})$,

$$\sum_{I_z=-1,0,1}\sum_{J_z=-2,\ldots,2} \left[O^{0,s_{\rm NL}}_{0,2,2,J_z,1,I_z}(\mathbf{n})\right]^\dagger O^{0,s_{\rm NL}}_{0,2,2,J_z,1,I_z}(\mathbf{n}), \tag{43}$$

the ${}^3D_1$ interaction $V_{4,{}^3D_1}(\mathbf{n})$,

$$\sum_{J_z=-1,0,1} \left[O^{0,s_{\rm NL}}_{1,2,1,J_z,0,0}(\mathbf{n})\right]^\dagger O^{0,s_{\rm NL}}_{1,2,1,J_z,0,0}(\mathbf{n}), \tag{44}$$

the ${}^3D_2$ interaction $V_{4,{}^3D_2}(\mathbf{n})$,

$$\sum_{J_z=-2,\ldots,2} \left[O^{0,s_{\rm NL}}_{1,2,2,J_z,0,0}(\mathbf{n})\right]^\dagger O^{0,s_{\rm NL}}_{1,2,2,J_z,0,0}(\mathbf{n}), \tag{45}$$

and the ${}^3D_3$ interaction $V_{4,{}^3D_3}(\mathbf{n})$,

$$\sum_{J_z=-3,\ldots,3} \left[O^{0,s_{\rm NL}}_{1,2,3,J_z,0,0}(\mathbf{n})\right]^\dagger O^{0,s_{\rm NL}}_{1,2,3,J_z,0,0}(\mathbf{n}). \tag{46}$$

At order Q^4 we also have the P-F mixing term $V_{4,PF}(\mathbf{n})$,

$$\sum_{I_z=-1,0,1}\sum_{J_z=-2,\ldots,2} \left[O^{0,s_{\rm NL}}_{1,3,2,J_z,0,0}(\mathbf{n})\right]^\dagger O^{0,s_{\rm NL}}_{1,1,2,J_z,0,0}(\mathbf{n}) + \sum_{I_z=-1,0,1}\sum_{J_z=-2,\ldots,2} \left[O^{0,s_{\rm NL}}_{1,1,2,J_z,0,0}(\mathbf{n})\right]^\dagger O^{0,s_{\rm NL}}_{1,3,2,J_z,0,0}(\mathbf{n}). \tag{47}$$

D. Isospin-breaking short-range interactions

We also include additional isospin-breaking ${}^1S_0$ contact interactions for proton-proton scattering ($I_z = 1$) and neutron-neutron scattering ($I_z = -1$). These are not relevant for neutron-proton scattering, but we nevertheless discuss the interactions for completeness. We define the two isospin-breaking interactions $V^{I_z=1}_{0,{}^1S_0}(\mathbf{n})$,

$$\left[O^{0,s_{\rm NL}}_{0,0,0,0,1,I_z=1}(\mathbf{n})\right]^\dagger O^{0,s_{\rm NL}}_{0,0,0,0,1,I_z=1}(\mathbf{n}), \tag{48}$$

and $V^{I_z=-1}_{0,{}^1S_0}(\mathbf{n})$,

$$\left[O^{0,s_{\rm NL}}_{0,0,0,0,1,I_z=-1}(\mathbf{n})\right]^\dagger O^{0,s_{\rm NL}}_{0,0,0,0,1,I_z=-1}(\mathbf{n}). \tag{49}$$

In terms of counting momenta, these are order Q^0. However, they are suppressed by the small size of the isospin-breaking coefficient. Following our previous analyses, we count this correction as order Q^2. We do not consider higher-order isospin breaking terms in this work, but they will be included in future studies.

V. LONG-RANGE INTERACTIONS

A. One-pion exchange

The one-pion exchange interaction $V_{\rm OPE}$ has the form

$$V_{\rm OPE} = -\frac{g_A^2}{8F_\pi^2} \sum_{\mathbf{n}',\mathbf{n},S',S,I} :\rho_{S',I}(\mathbf{n}')f_{S'S}(\mathbf{n}'-\mathbf{n})\rho_{S,I}(\mathbf{n}):, \tag{50}$$

where $f_{S'S}$ is defined as

$$f_{S'S}(\mathbf{n}'-\mathbf{n}) = \frac{1}{L^3}\sum_{\mathbf{q}} \frac{Q(q_{S'})Q(q_S)\exp\left[-i\mathbf{q}\cdot(\mathbf{n}'-\mathbf{n})-b_\pi\left(\mathbf{q}^2+M_\pi^2\right)\right]}{\mathbf{q}^2+M_\pi^2}, \tag{51}$$

where L is the length of the cubic periodic box and each lattice momentum component q_S is an integer multiplied by $2\pi/L$.

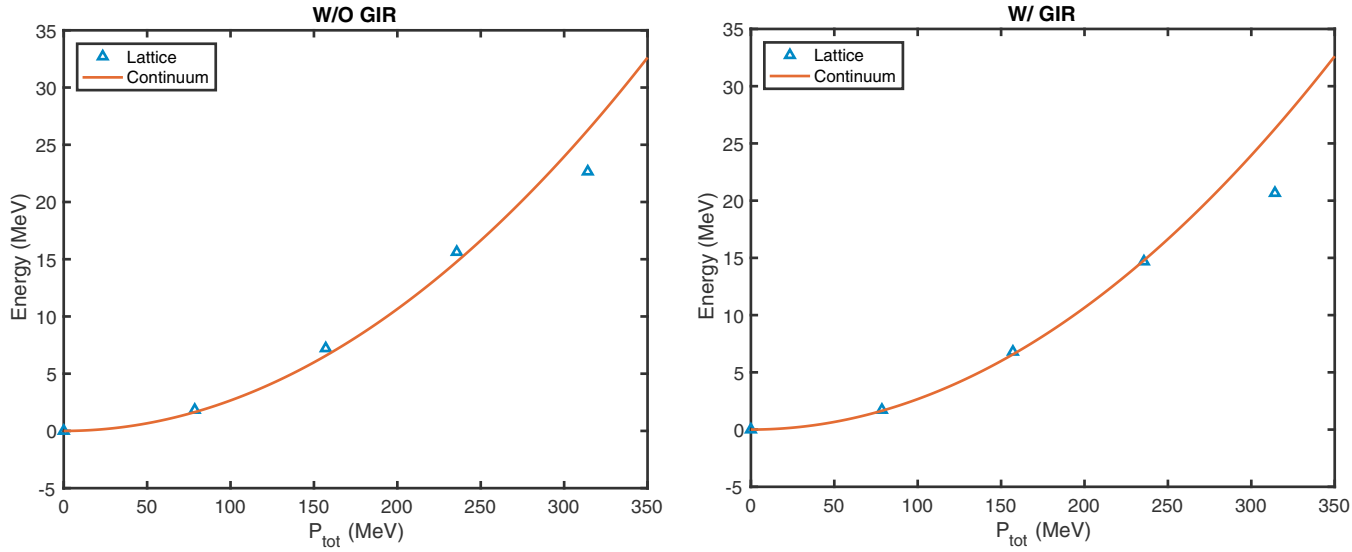

FIG. 1. Dispersion relation of the deuteron. Left: Without any Galilean invariance restoration (GIR). Right: With GIR as provided by the operator $V_{\rm GIR}$ with coefficient $C_{\rm GIR} = -0.0658$.

The function $Q(q_S)$ is defined as

$$Q(q_S) = \tfrac{3}{2}\sin(q_S) - \tfrac{3}{10}\sin(2q_S) + \tfrac{1}{30}\sin(3q_S), \qquad (52)$$

which equals q_S up to a correction of order q_S^7. The parameter b_π is included to remove short-distance lattice artifacts in the one-pion exchange interaction. In the present calculation, we set $b_\pi = 0.25$ in lattice units. We have used the combination $\mathbf{q}^2 + M_\pi^2$ in the exponential as suggested in recent work [12] as a momentum-space regulator that does not affect the long-distance behavior. At leading order we take the pion mass to be the mass of the neutral pion, $M_\pi = M_\pi^0 = M_{\pi,I=3}$.

B. Two-pion exchange

The cutoff momentum arising from the lattice regularization is $\Lambda_{\rm latt} = \pi/a$, with a the spatial lattice spacing. For coarse lattice spacings such as $a = 1.97$ fm and $a = 1.64$ fm, the corresponding lattice cutoffs are 314 and 377 MeV,

TABLE I. Low-energy constants determined by N^{3}LO fits using lattice spacings $a = 1.97$, 1.64, 1.32, and 0.99 fm. For calculations using $a = 1.32$ and 0.99 fm, full NN interactions are used. All LECs are given in lattice units.

LEC	$a = 1.97$ fm	$a = 1.64$ fm	$a = 1.32$ fm	$a = 0.99$ fm
$C_{0,^1S_0}$	0.1050 ± 0.0006	0.0879 ± 0.0004	0.0833 ± 0.0010	0.0860 ± 0.0004
$C_{0,^3S_1}$	0.0256 ± 0.0056	0.0322 ± 0.0031	0.0455 ± 0.0289	0.0520 ± 0.0006
$C_{2,^1S_0}$	0.0217 ± 0.0002	0.0242 ± 0.0002	0.0271 ± 0.0007	0.0256 ± 0.0005
$C_{2,^3S_1}$	0.0267 ± 0.0020	0.0280 ± 0.0014	0.0310 ± 0.0179	0.0263 ± 0.0005
$C_{2,SD}$	−0.0605 ± 0.0041	−0.0421 ± 0.0047	−0.0291 ± 0.0137	−0.0089 ± 0.0021
$C_{2,^1P_1}$	0.1930 ± 0.0012	0.1758 ± 0.0013	0.1469 ± 0.0003	0.1321 ± 0.0002
$C_{2,^3P_0}$	−0.0084 ± 0.0004	0.0190 ± 0.0007	0.0495 ± 0.0004	0.0940 ± 0.0003
$C_{2,^3P_1}$	0.1332 ± 0.0013	0.1217 ± 0.0007	0.1186 ± 0.0034	0.1300 ± 0.0007
$C_{2,^3P_2}$	0.0441 ± 0.0001	0.0461 ± 0.0018	0.0584 ± 0.0021	0.0665 ± 0.0002
$C_{4,^1S_0}$	0.0073 ± 0.0001	0.0081 ± 0.0001	0.0108 ± 0.0005	0.0148 ± 0.0006
$C_{4,^3S_1}$	0.0079 ± 0.0007	0.0081 ± 0.0006	0.0119 ± 0.0109	0.0153 ± 0.0004
$C_{4,SD}$	0.0005 ± 0.0003	−0.0011 ± 0.0006	−0.0026 ± 0.0029	−0.0098 ± 0.0011
$C_{4,^1P_1}$	−0.0004 ± 0.0006	−0.0057 ± 0.0006	−0.0104 ± 0.0001	−0.0105 ± 0.0002
$C_{4,^3P_0}$	−0.0001 ± 0.0002	−0.0006 ± 0.0005	−0.0024 ± 0.0001	−0.0022 ± 0.0007
$C_{4,^3P_1}$	−0.0006 ± 0.0004	−0.0004 ± 0.0004	−0.0019 ± 0.0013	0.0063 ± 0.0013
$C_{4,^3P_2}$	0.0080 ± 0.0002	0.0090 ± 0.0012	0.0105 ± 0.0008	0.0078 ± 0.0003
$C_{4,PF}$	0.0072 ± 0.0002	0.0041 ± 0.0011	0.0017 ± 0.0002	0.0026 ± 0.0002
$C_{4,^1D_2}$	0.0105 ± 0.0006	0.0088 ± 0.0005	0.0136 ± 0.0001	0.0190 ± 0.0050
$C_{4,^3D_1}$	0.0327 ± 0.0023	0.0319 ± 0.0039	0.0318 ± 0.0134	0.0720 ± 0.0122
$C_{4,^3D_2}$	−0.032 ± 0.0017	−0.0324 ± 0.0019	−0.0187 ± 0.0022	−0.0005 ± 0.0014
$C_{4,^3D_3}$	0.0030 ± 0.0026	0.0088 ± 0.0027	0.0059 ± 0.0013	0.0127 ± 0.0041

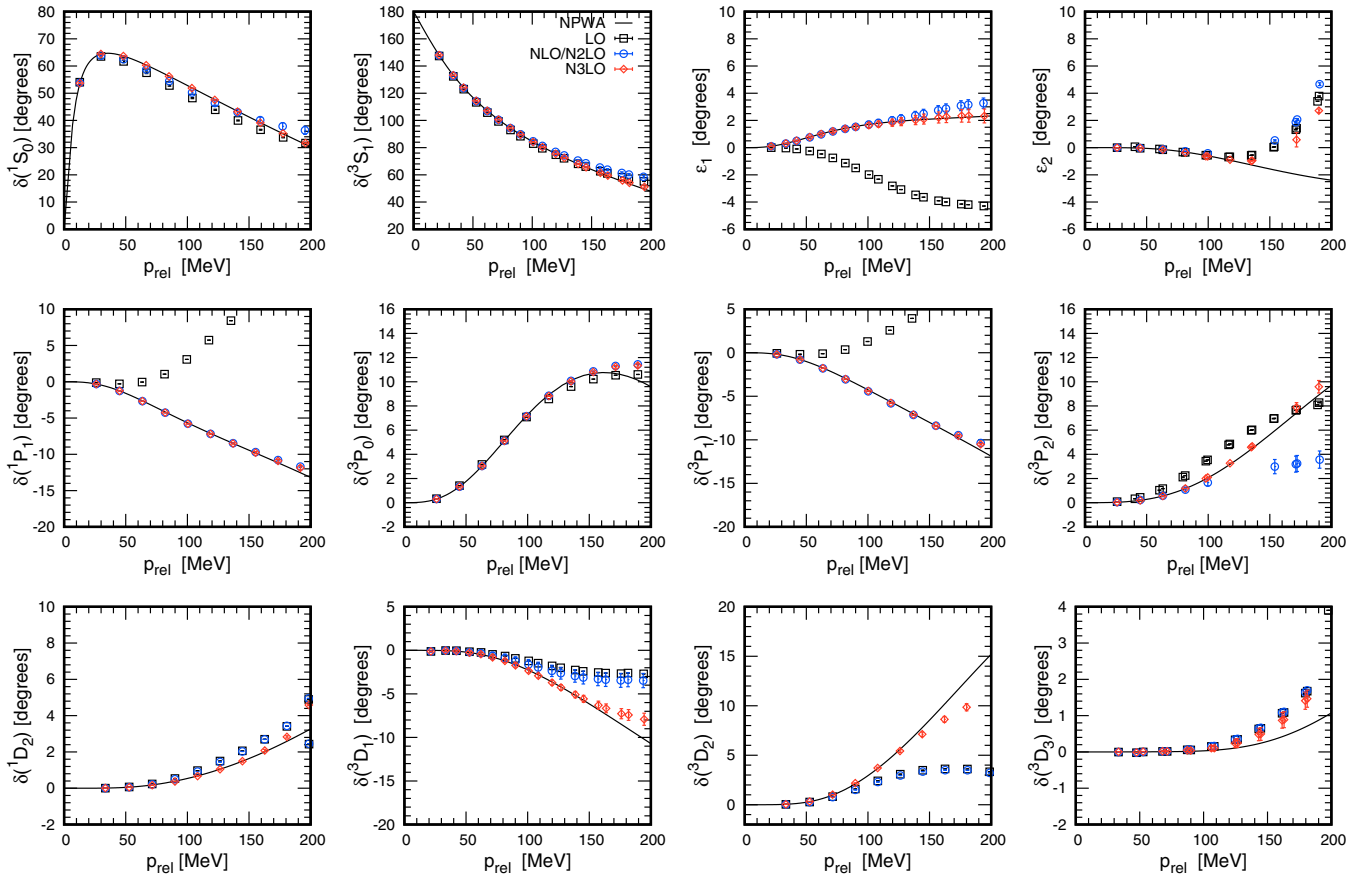

FIG. 2. Neutron-proton scattering phase shifts and mixing angles versus relative momenta. The lattice spacing $a = 1.97$ fm is used. The TPEP is not included explicitly as discussed in the text.

respectively. For momenta lying below these cutoff scales, the two-pion-exchange potential (TPEP) can be expanded in powers of $\mathbf{q}^2/(4\pi^2)$, resulting in operators that are exactly the same as our short-range contact terms. We conclude that the TPEP at coarse lattice spacings can be replaced by retuning the low-energy constants (LECs) for these contact terms [13]. For these two coarse lattice spacings, the TPEP does not have observable effects but only changes the LECs.

For the two smaller lattice spacings, $a = 1.32$ fm and $a = 0.99$ fm, however, higher momenta can be reached and the structure of the two-pion-exchange potential can be resolved. In these cases we include the TPEP explicitly. According to the power counting of chiral EFT, the TPEP first appears at order $O(Q^2)$ or NLO, the subleading TPEP appears at order $O(Q^3)$ or N^{2}LO, and so on [14]. Similarly to what we do to the one-pion exchange potential, we also regularize the TPEP by a Gaussian form factor in momentum space,

$$F(\boldsymbol{q}) = \exp\left[-b_\pi\left(\boldsymbol{q}^2 + M_\pi^2\right)\right] = \exp\left[-\frac{\boldsymbol{q}^2 + M_\pi^2}{\Lambda^2}\right], \qquad (53)$$

where $\Lambda = 1/\sqrt{b_\pi}$ [12]. In the present calculation, we set $b_\pi = 0.25$ l.u., which equates to $\Lambda = 300$ MeV for $a = 1.32$ fm and $\Lambda = 400$ MeV for $a = 0.99$ fm. In this work, the relativistic corrections stemming from the $1/m_N^2$ corrections to the one-pion exchange potential and $1/m_N$ correction to the TPEP at order $O(Q^4)$ are not taken into account.

The TPEP up to order $O(Q^4)$ or N^{3}LO is completely local and can be written in the form

$$\begin{aligned} V_{\rm TPEP} &= V_{\rm TPEP}^{Q^2} + V_{\rm TPEP}^{Q^3} + V_{\rm TPEP}^{Q^4} \\ &= \frac{1}{2}\sum_{\mathbf{n},\mathbf{n}'} :\rho(\mathbf{n})V_C(\mathbf{n}-\mathbf{n}')\rho(\mathbf{n}'): + \frac{1}{2}\sum_{I}\sum_{\mathbf{n},,\mathbf{n}'} :\rho_I(\mathbf{n})W_C(\mathbf{n}-\mathbf{n}')\rho_I(\mathbf{n}'): \\ &+ \frac{1}{2}\sum_{S}\sum_{\mathbf{n},\mathbf{n}'} :\rho_S(\mathbf{n})V_\sigma(\mathbf{n}-\mathbf{n}')\rho_S(\mathbf{n}'): + \frac{1}{2}\sum_{S,I}\sum_{\mathbf{n},\mathbf{n}'} :\rho_{S,I}(\mathbf{n})W_\sigma(\mathbf{n}-\mathbf{n}')\rho_{S,I}(\mathbf{n}'): \\ &+ \frac{1}{2}\sum_{S_1,S_2}\sum_{\mathbf{n},\mathbf{n}'} :\rho_{S_1}(\mathbf{n})(V_T)_{S_1,S_2}(\mathbf{n}-\mathbf{n}')\rho_{S_2}(\mathbf{n}'): + \frac{1}{2}\sum_{S_1,S_2,I}\sum_{\mathbf{n},\mathbf{n}'} :\rho_{S_1,I}(\mathbf{n})(W_T)_{S_1,S_2}(\mathbf{n}-\mathbf{n}')\rho_{S_2,I}(\mathbf{n}'):, \end{aligned} \qquad (54)$$

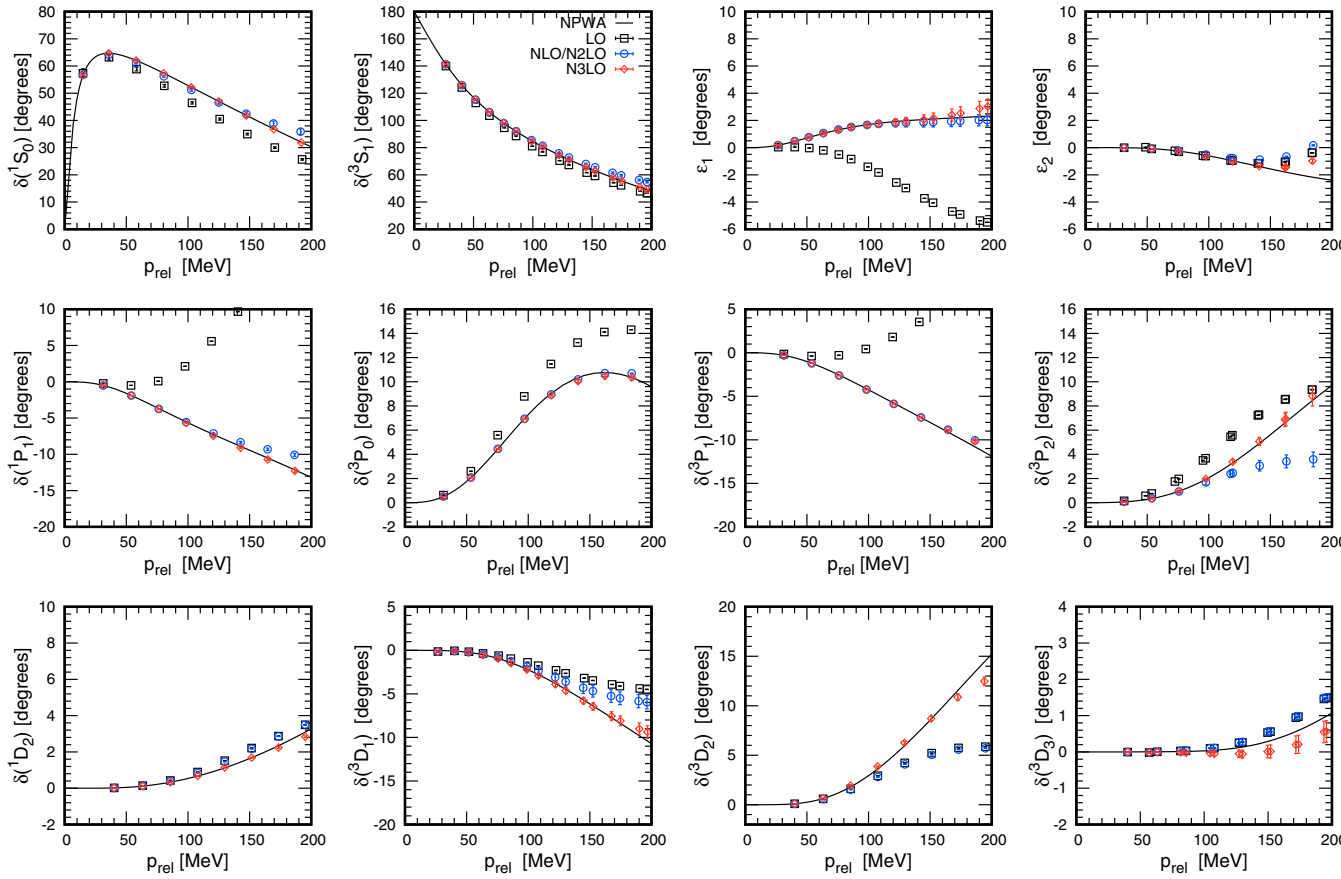

FIG. 3. Neutron-proton scattering phase shifts and mixing angles versus relative momenta. The lattice spacing $a = 1.64$ fm is used. The TPEP is not included explicitly as discussed in the text.

where $V_{C/\sigma}$, $(V_T)_{S_1,S_2}$, $W_{C/\sigma}$, and $(W_T)_{S_1,S_2}$ are scalar functions in the coordinate space, and

$$V_{C/\sigma}(\mathbf{n}-\mathbf{n}') = \frac{1}{L^3}\sum_{\mathbf{q}} \exp[-i\mathbf{q}\cdot(\mathbf{n}-\mathbf{n}')]V_{C/\sigma}(\mathbf{q})F(\mathbf{q}), \tag{55}$$

$$W_{C/\sigma}(\mathbf{n}-\mathbf{n}') = \frac{1}{L^3}\sum_{\mathbf{q}} \exp[-i\mathbf{q}\cdot(\mathbf{n}-\mathbf{n}')]W_{C/\sigma}(\mathbf{q})F(\mathbf{q}), \tag{56}$$

$$(V_T)_{S_1,S_2}(\mathbf{n}-\mathbf{n}') = \frac{1}{L^3}\sum_{\mathbf{q}} \exp[-i\mathbf{q}\cdot(\mathbf{n}-\mathbf{n}')](V_T)_{S_1,S_2}(\mathbf{q})F(\mathbf{q})Q(q_{S_1})Q(q_{S_2}), \tag{57}$$

$$(W_T)_{S_1,S_2}(\mathbf{n}-\mathbf{n}') = \frac{1}{L^3}\sum_{\mathbf{q}} \exp[-i\mathbf{q}\cdot(\mathbf{n}-\mathbf{n}')](W_T)_{S_1,S_2}(\mathbf{q})F(\mathbf{q})Q(q_{S_1})Q(q_{S_2}). \tag{58}$$

The definitions for the functions $V_{C/\sigma}(\mathbf{q})$, $(W_T)_{C/\sigma}(\mathbf{q})$, $(V_T)_{S_1,S_2}(\mathbf{q})$, and $(W_T)_{S_1,S_2}(\mathbf{q})$ are given in Refs. [12,15–18].

C. Coulomb and long-range strong isospin breaking

The Coulomb interaction will not be relevant for neutron-proton scattering, but we nevertheless discuss it here for completeness. The Coulomb interaction can be written as

$$V_{\text{Coulomb}} = -\frac{\alpha_{\text{EM}}}{2}\sum_{\mathbf{n}',\mathbf{n}} : \frac{1}{4}[\rho(\mathbf{n}') + \rho_{I=3}(\mathbf{n}')]\frac{1}{d(\mathbf{n}'-\mathbf{n})}[\rho(\mathbf{n}) + \rho_{I=3}(\mathbf{n})] :, \tag{59}$$

where $d(\mathbf{n}'-\mathbf{n})$ is the shortest length of $\mathbf{n}'$-$\mathbf{n}$ as measured on the periodic lattice, and we define the value of d at the origin to be $1/2$. Our notation $\rho_{I=3}$ refers to the $I = 3$ isospin component of ρ_I.

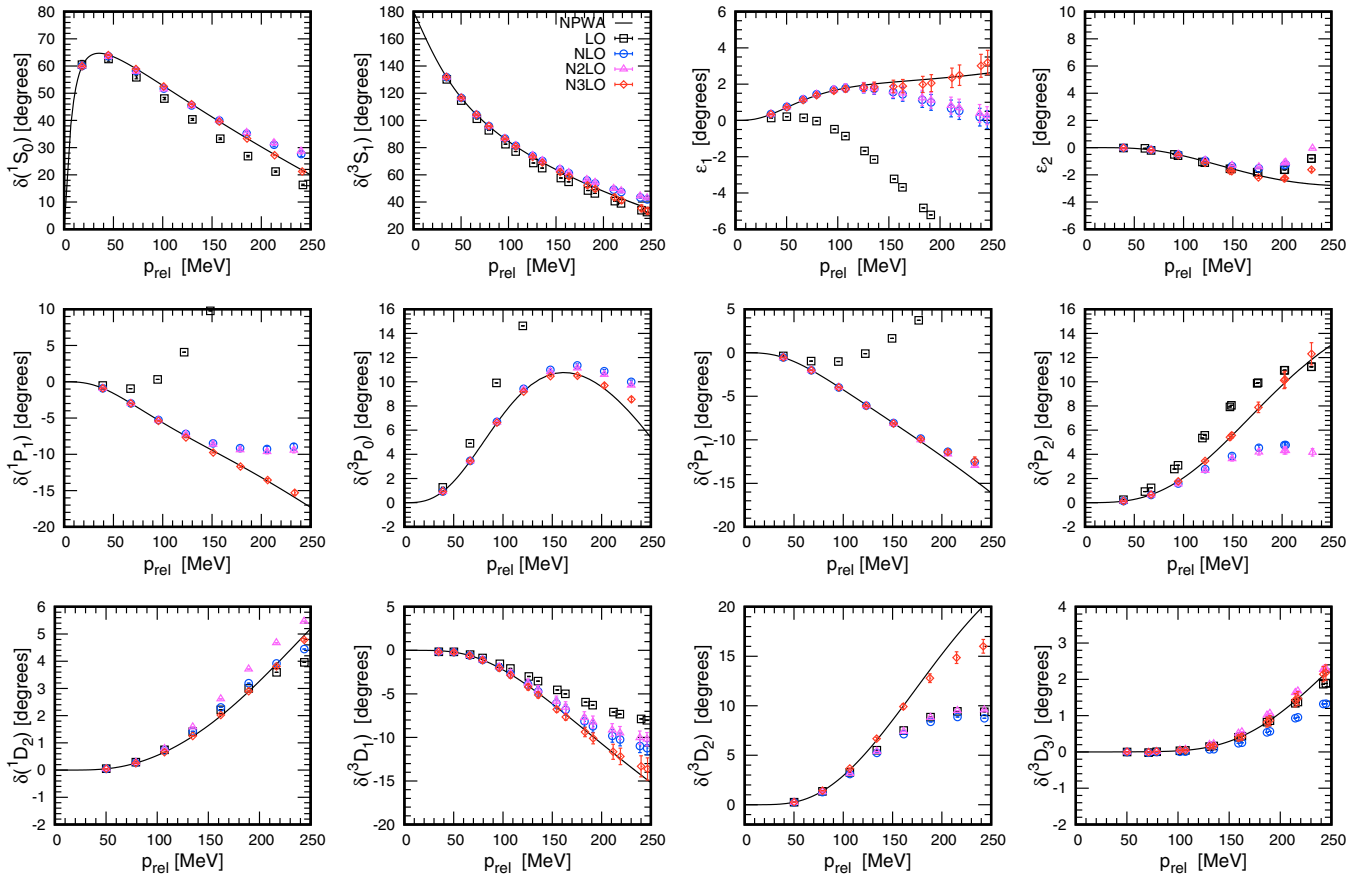

FIG. 4. Neutron-proton scattering phase shifts and mixing angles versus relative momenta. The lattice spacing $a = 1.32$ fm and full NN interactions are used.

The long-range isospin-breaking correction, due to differences in the charged and neutral pion mass in one-pion exchange, has the form

$$V_{\rm OPE}^{\rm IB} = -\frac{g_A^2}{8f_\pi^2} \sum_{\mathbf{n}',\mathbf{n},S',S,I} :\rho_{S',I}(\mathbf{n}')f_{S'SI}^{\rm IB}(\mathbf{n}'-\mathbf{n})\rho_{S,I}(\mathbf{n}):, \tag{60}$$

where $f_{S'SI}^{\rm IB}$ is defined as

$$f_{S'SI}^{\rm IB}(\mathbf{n}'-\mathbf{n}) = \frac{1}{L^3}\sum_{\mathbf{q}} \frac{Q(q_{S'})Q(q_S)\exp\left[-i\mathbf{q}\cdot(\mathbf{n}'-\mathbf{n}) - b_\pi\left(\mathbf{q}^2+M_{\pi,I}^2\right)\right]}{\mathbf{q}^2+M_{\pi,I}^2} - f_{S'S}(\mathbf{n}'-\mathbf{n}), \tag{61}$$

where $M_{\pi,1} = M_{\pi,2} = M_\pi^+ = M_\pi^-$ and $M_{\pi,3} = M_\pi^0$. As in previous analyses we count this correction as order Q^2.

VI. GALILEAN INVARIANCE RESTORATION (GIR)

Galilean invariance is the statement that the laws of Newtonian physics for a nonrelativistic system are independent of the velocity of the center of mass. In a lattice regularized system, however, the effect of the cutoff is different in moving frames, and this leads to the breaking of Galilean invariance [19]. There is also some breaking of Galilean invariance caused by the nonlocal smearing parameter $s_{\rm NL}$ that we use in the construction of our interactions. This arises from the residual dependence of the interactions on the velocity of the center of mass. Fortunately, in many cases of interest these two Galilean invariance breaking effects have the tendency to partially cancel.

In order to restore Galilean invariance in the two-nucleon system, we include the two-nucleon nearest-neighbor hopping operator,

$$V_{\rm GIR} = V_{\rm GIR}^0 + V_{\rm GIR}^1, \tag{62}$$

where

$$V_{\rm GIR}^0 = C_{\rm GIR} \sum_{\mathbf{n},i,j,i',j'} a_{i,j}^\dagger(\mathbf{n})a_{i',j'}^\dagger(\mathbf{n})a_{i',j'}(\mathbf{n})a_{i,j}(\mathbf{n}) \tag{63}$$

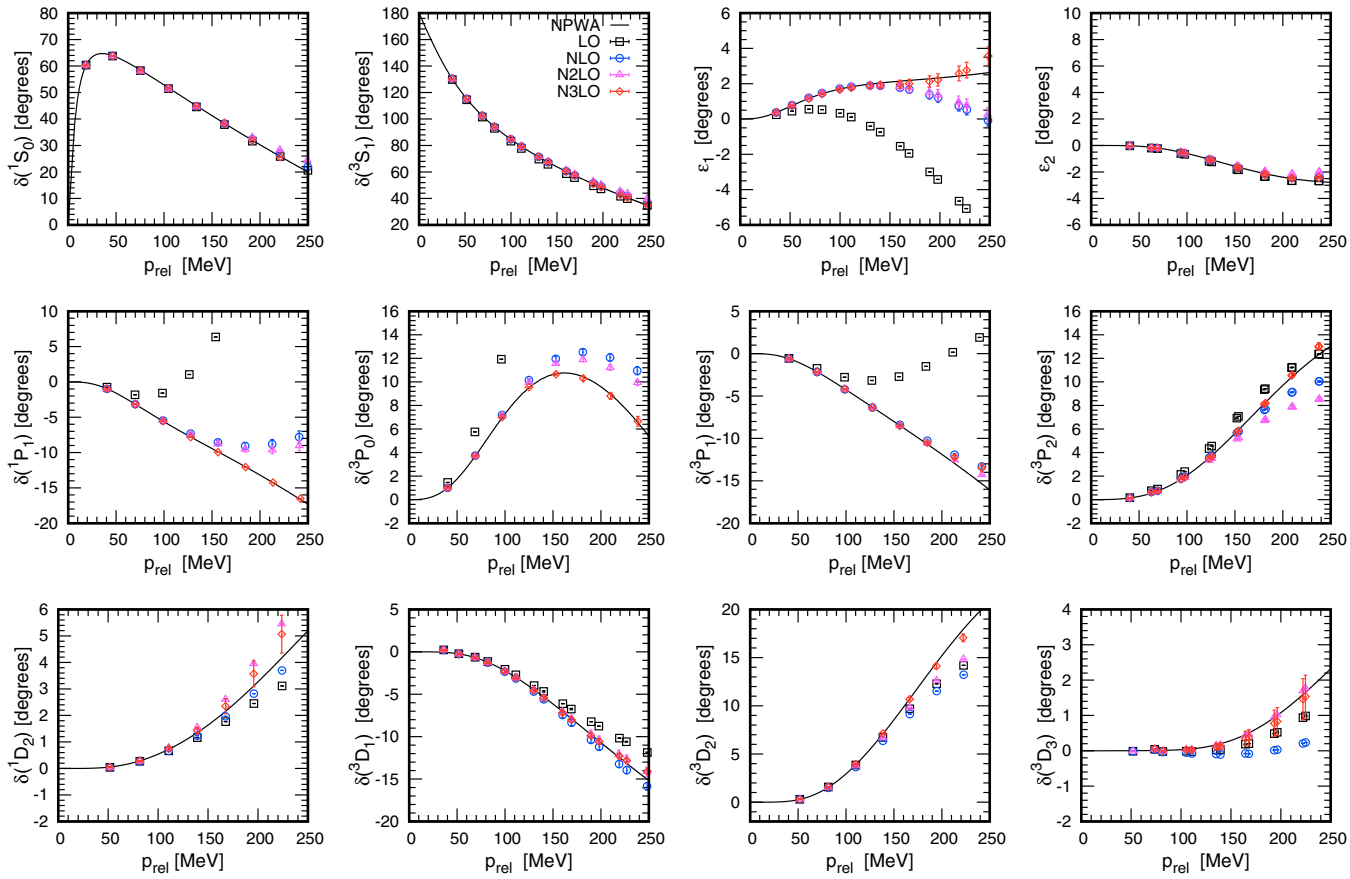

FIG. 5. Neutron-proton scattering phase shifts and mixing angles versus relative momenta. The lattice spacing $a = 0.99$ fm and full NN interactions are used.

and

$$V^1_{\rm GIR} = -\frac{C_{\rm GIR}}{6} \sum_{\mathbf{n},i,j,i',j'} \sum_{\mathbf{n}'} a^\dagger_{i,j}(\mathbf{n}+\mathbf{n}')a^\dagger_{i',j'}(\mathbf{n}+\mathbf{n}')a_{i',j'}(\mathbf{n})a_{i,j}(\mathbf{n}). \tag{64}$$

Let us write $|\mathbf{P}_{\rm tot}\rangle$ as a two-body bound-state wave function with total momentum $\mathbf{P}_{\rm tot}$. We note that

$$\langle \mathbf{P}_{\rm tot}|V^0_{\rm GIR}|\mathbf{P}_{\rm tot}\rangle \tag{65}$$

is independent of $\mathbf{P}_{\rm tot}$, and so we have

$$\langle \mathbf{P}_{\rm tot}|V^0_{\rm GIR}|\mathbf{P}_{\rm tot}\rangle = \langle \mathbf{0}|V^0_{\rm GIR}|\mathbf{0}\rangle, \tag{66}$$

where $|\mathbf{0}\rangle$ is the two-body bound-state wave function with zero total momentum. Furthermore,

$$\langle \mathbf{P}_{\rm tot}|V^1_{\rm GIR}|\mathbf{P}_{\rm tot}\rangle = -\frac{1}{6}\langle \mathbf{0}|V^0_{\rm GIR}|\mathbf{0}\rangle \sum_{\mathbf{n}'} e^{-i\mathbf{P}_{\rm tot}\cdot\vec{\mathbf{n}}'} = \left[-\frac{1}{3}\cos(P_{{\rm tot},1}) - \frac{1}{3}\cos(P_{{\rm tot},2}) - \frac{1}{3}\cos(P_{{\rm tot},3})\right]\langle \mathbf{0}|V^0_{\rm GIR}|\mathbf{0}\rangle. \tag{67}$$

Therefore

$$\langle \mathbf{P}_{\rm tot}|V_{\rm GIR}|\mathbf{P}_{\rm tot}\rangle = \left[1 - \tfrac{1}{3}\cos(P_{{\rm tot},1}) - \tfrac{1}{3}\cos(P_{{\rm tot},2}) - \tfrac{1}{3}\cos(P_{{\rm tot},3})\right]\langle \mathbf{0}|V^0_{\rm GIR}|\mathbf{0}\rangle. \tag{68}$$

In this manner we can restore Galilean invariance up to order Q^2 by tuning the coefficient of $V_{\rm GIR}$ according to the dispersion relation of the deuteron and the ${}^1S_0$ ground state at finite volume. The deuteron dispersion relation is far more useful for this purpose, however, since the ${}^1S_0$ ground state is a continuum state that shows negligible Galilean invariance breaking in its dispersion relation. This is true for all continuum states, and this is why the amount of Galilean invariance breaking seen in the higher partial waves is also negligible. We will consider Galilean invariance breaking effects beyond order Q^2 in future work.

As an example of how to determine the Galilean invariance restoration operator coefficient, we show the results for lattice spacing $a = 1.97$ fm in Fig. 1. The left and right panels are the deuteron dispersion relations before and after including the GIR operator, respectively. We see that the amount of correction is relatively small. The fitted coefficient for $V_{\rm GIR}$ is found to be $C_{\rm GIR} = -0.0658$. The amount of Galilean invariance breaking is somewhat smaller than this for the smaller lattice spacings.

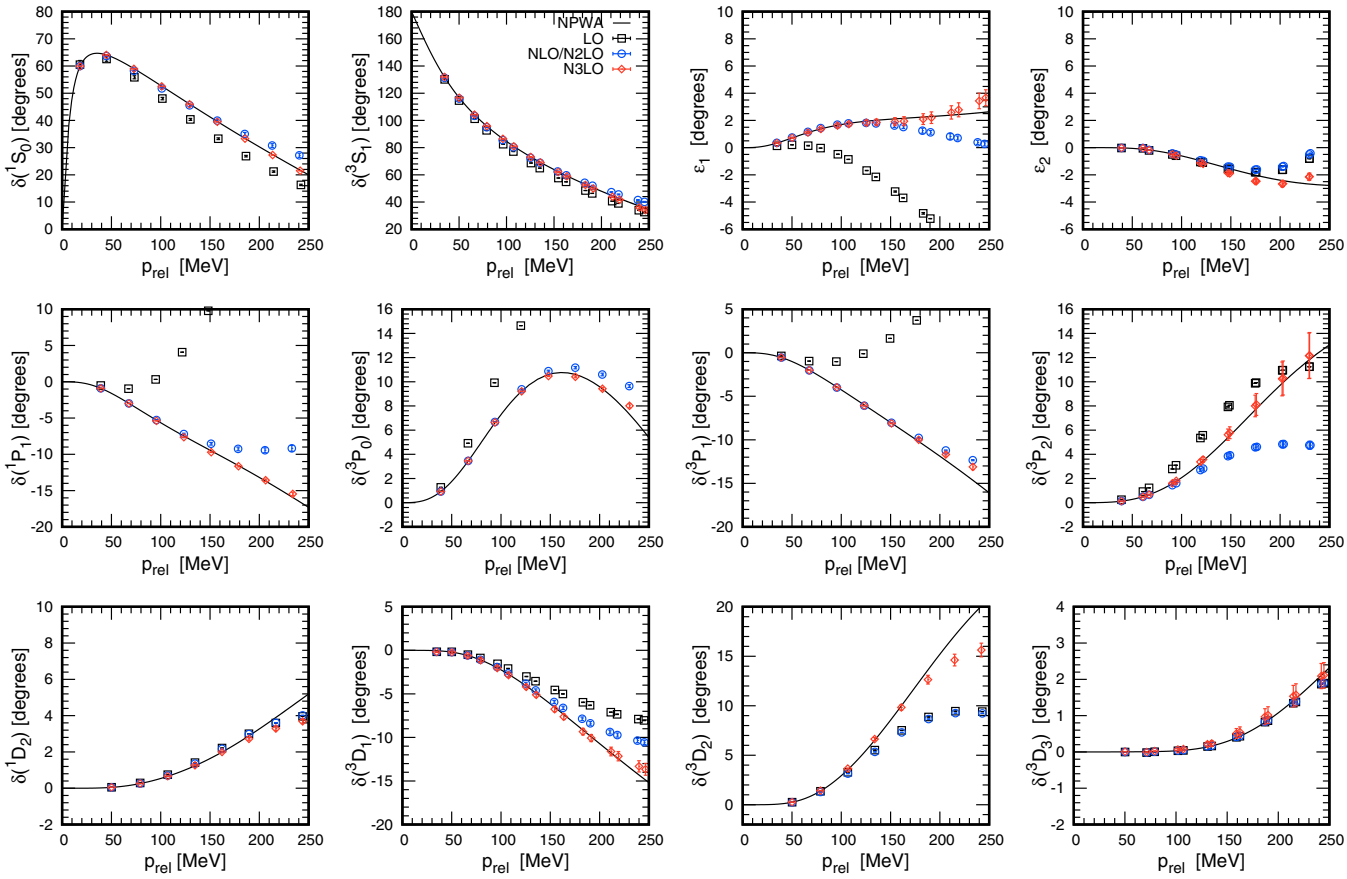

FIG. 6. Neutron-proton scattering phase shifts and mixing angles versus relative momenta. The lattice spacing $a = 1.32$ fm is used. The TPEP is not included in this case for comparison.

VII. SCATTERING ON THE LATTICE

In order to calculate the scattering phase shifts and mixing angles, we first construct radial wave functions through the spherical harmonics with quantum numbers (L, L_z) [20,21],

$$|r\rangle^{L,L_z} = \sum_{\mathbf{r}'} Y_{L,L_z}(\hat{r}')\delta_{|\mathbf{r}'|=r}|\mathbf{r}'\rangle, \tag{69}$$

where $\mathbf{r}'$ runs over all lattice grid points having the same radial lattice distance. We group together data into a large number of radial bins so that in each bin, $r - \delta r/2 < |\mathbf{r}'| < r + \delta r/2$, with a very small width parameter δr. Using this definition of the radial wave function, the Hamiltonian matrix over a three-dimensional lattice can be reduced to a one-dimensional radial Hamiltonian, $H_{\mathbf{r},\mathbf{r}'} \to H_{r,r'}$.

We follow the method described in Ref. [20], which uses an auxiliary radial potential. We extract the phase shifts as well as the mixing angles from the radial wave functions in the region where the NN force and auxiliary potentials are vanishing. In this range, the wave function has the form

$$A_L h_L^-(kr) - B_L h_L^+(kr), \tag{70}$$

where $h_L^-(kr)$ and $h_L^+(kr)$ are the spherical Bessel functions, $k = \sqrt{2\mu E}$, μ is the reduced mass, and E is the energy. The scattering coefficients A_L and B_L satisfy the relations

$$B_L = S_L A_L, \tag{71}$$

where $S_L = \exp(2i\delta_L)$ is the S matrix and δ_L is the phase shift. The phase shift is determined by setting

$$\delta_L = \frac{1}{2i}\log\left(\frac{B_L}{A_L}\right). \tag{72}$$

In the case of the coupled channels with $J > 0$, both of the coupled partial waves, $L = J - 1$ and $L = J + 1$, satisfy Eq. (71), and the S matrix couples the two channels together. Throughout this work we adopt the so-called Stapp parametrization of the phase shifts and mixing angles for the coupled channels [22],

$$S = \begin{bmatrix} \cos(2\epsilon)\exp\left(2i\delta_{J-1}^{1J}\right) & i\sin(2\epsilon)\exp\left(i\delta_{J-1}^{1J} + i\delta_{J+1}^{1J}\right) \\ i\sin 2\epsilon\exp\left(i\delta_{J-1}^{1J} + i\delta_{J+1}^{1J}\right) & \cos(2\epsilon)\exp\left(2i\delta_{J+1}^{1J}\right) \end{bmatrix}. \tag{73}$$

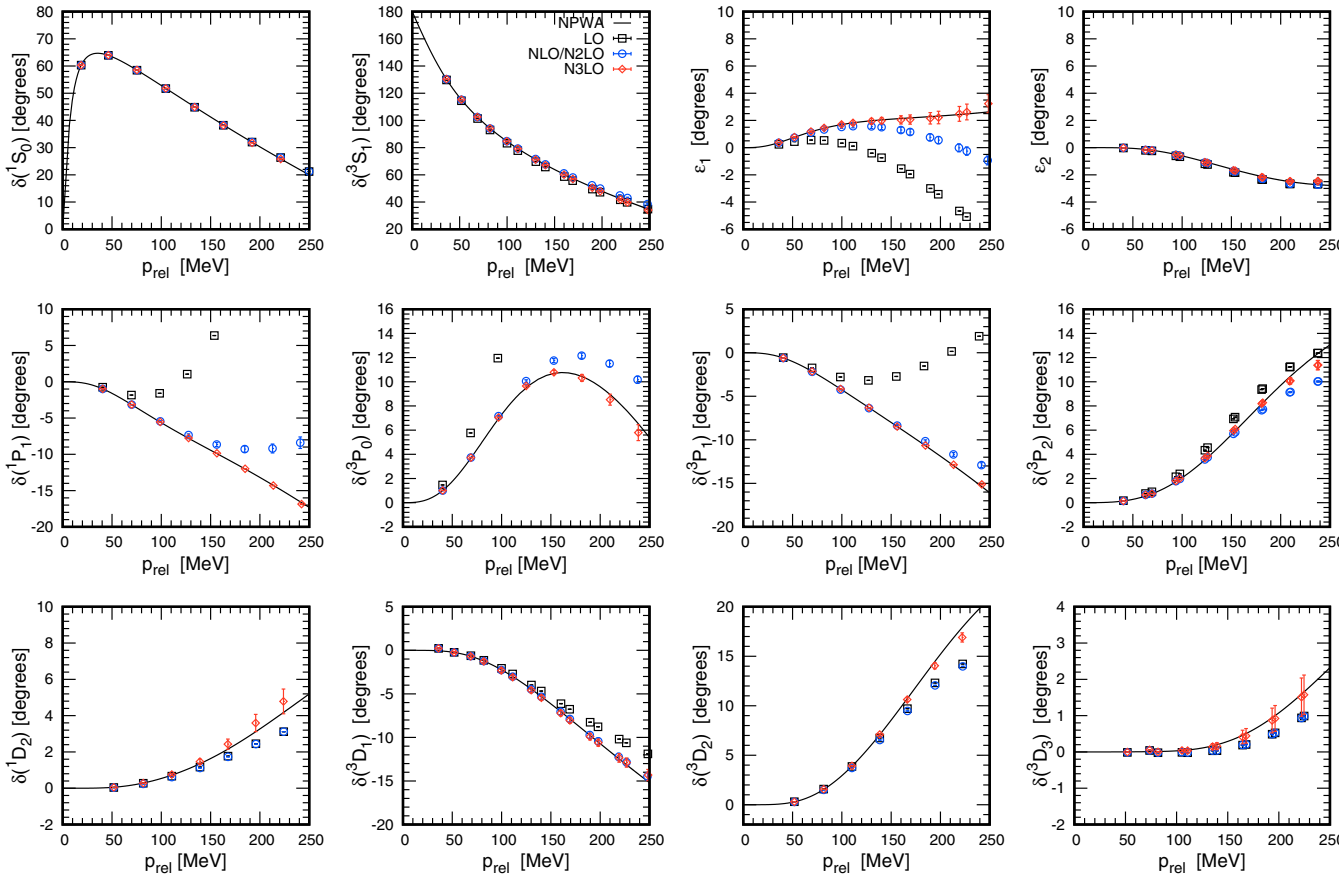

FIG. 7. Neutron-proton scattering phase shifts and mixing angles versus relative momenta. The lattice spacing $a = 0.99$ fm is used. The TPEP is not included in this case for comparison.

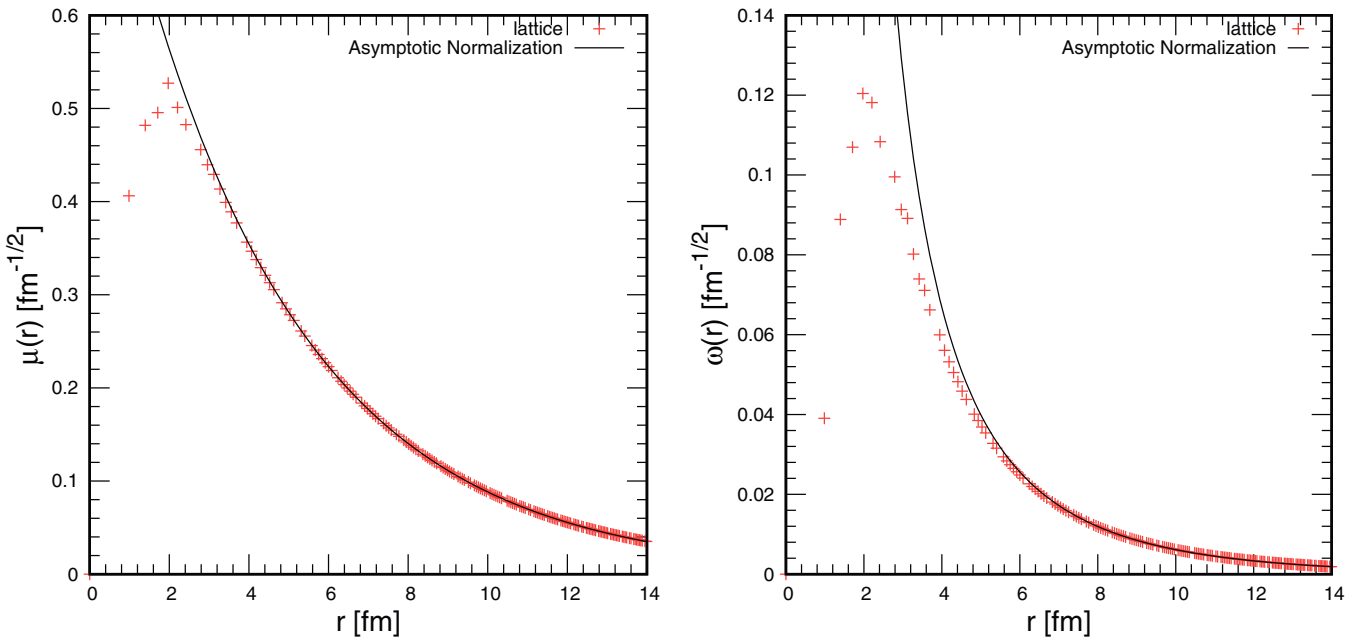

FIG. 8. Radial wave functions of the deuteron and its asymptotic behavior at large r. Wave functions are calculated using $a = 0.99$ fm with the full NN interaction up to order $O(Q^4)$. Left: S wave. Right: D wave.

TABLE II. Deuteron properties and S-wave parameters calculated with the full NN interaction up to chiral order $O(Q^4)$ using $a = 0.99$ fm. Errors we list here indicate uncertainties from the fitting procedure only.

	LO	NLO	N^{2}LO	N^{3}LO	Empirical
E_d (MeV)	2.2246 ± 0.0002	2.224575 ± 0.000016	2.224575 ± 0.000025	2.224575 ± 0.000011	2.224575(9) [24]
A_s (fm$^{-1/2}$)	0.8662 ± 0.0007	0.8772 ± 0.0003	0.8777 ± 0.0004	0.8785 ± 0.0004	0.8846(9) [25]
η	0.0212 ± 0.0000	0.0258 ± 0.0001	0.0257 ± 0.0002	0.0254 ± 0.0001	0.0256(4) [26]
Q_d (fm^2)	0.2134 ± 0.00000	0.2641 ± 0.0016	0.2623 ± 0.0023	0.2597 ± 0.0013	0.2859(3) [27]
r_d (fm)	1.9660 ± 0.0001	1.9548 ± 0.0005	1.9555 ± 0.0008	1.9545 ± 0.0005	1.97535(85) [28]
$a_{^3S_1}$	5.461 ± 0.000	5.415 ± 0.001	5.421 ± 0.002	5.417 ± 0.001	5.424(4) [29]
$r_{^3S_1}$	1.831 ± 0.0003	1.759 ± 0.002	1.760 ± 0.003	1.758 ± 0.002	1.759(5) [29]
$a_{^1S_0}$	−23.8 ± 0.1	−23.69 ± 0.05	−23.8 ± 0.2	−23.678 ± 0.038	−23.748(10) [29]
$r_{^1S_0}$	2.666 ± 0.001	2.647 ± 0.003	2.69 ± 0.02	2.647 ± 0.004	2.75(5) [29]
P_D (%)	1.92	3.48	3.41	3.36	

VIII. RESULTS FOR THE NEUTRON-PROTON PHASE SHIFTS

Different lattice spacings introduce different lattice artifacts. We make calculations using four lattice spacings, $a = 1.97$, 1.64, 1.32, and 0.99 fm to study the lattice spacing effects. We choose these values because the corresponding lattice momentum cutoffs, $\Lambda_{\rm latt} = \pi/a$, remain below the estimated breakdown scale of chiral effective field theory and the order-by-order convergence has been demonstrated to be favorable in few-body and many-body calculations. As noted in the discussion above, we do not include the TPEP for the two coarse lattice spacings, $a = 1.97$ and 1.64 fm. For the two smaller lattice spacings, $a = 1.32$ and 0.99 fm, we present results both with and without the TPEP in order to discern the effect of the TPEP.

In previous lattice studies we had to contend with interactions that had an effect in all channels. With these new lattice interactions this problem is now completely solved. We need

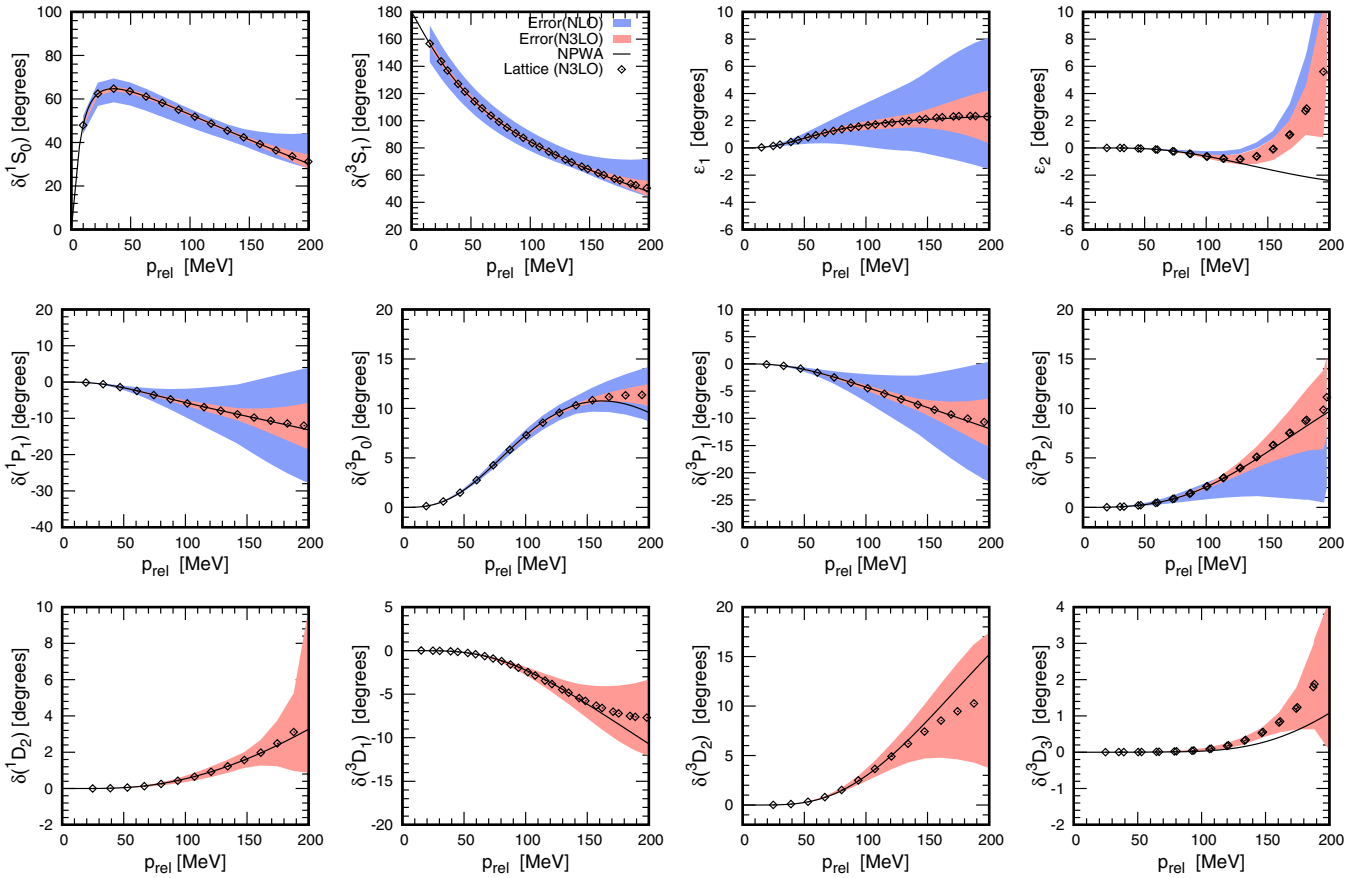

FIG. 9. Theoretical error bands for neutron-proton scattering phase shifts and mixing angles versus relative momenta for $a = 1.97$ fm. Blue and red bands signify the estimated uncertainties at NLO and N^{3}LO, respectively. The black solid line and diamonds denote the phase shift or mixing angle from the Nijmegen partial-wave analysis (NPWA) and lattice calculation at N^{3}LO, respectively.

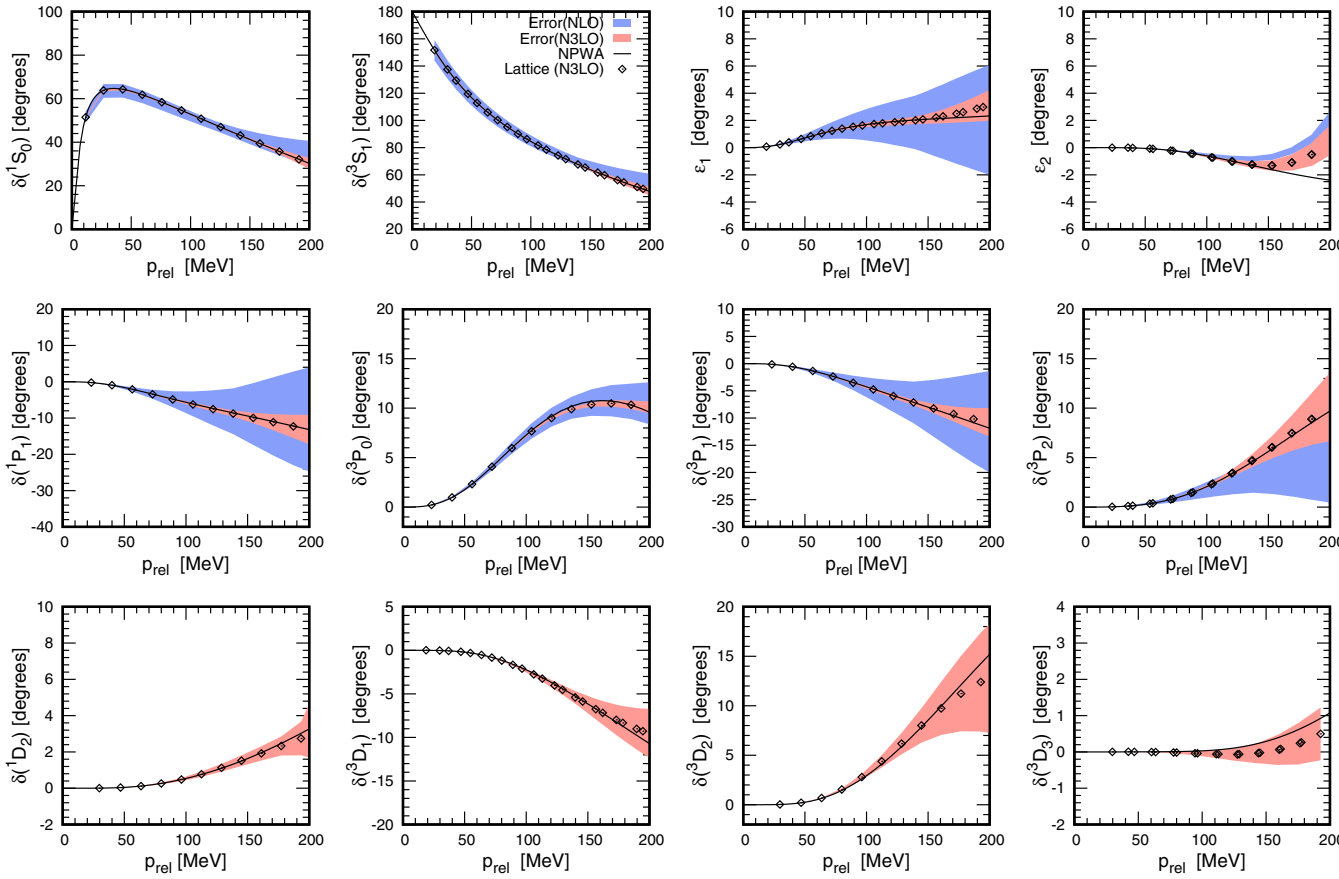

FIG. 10. Theoretical error bands for neutron-proton scattering phase shifts and mixing angles versus relative momenta for $a = 1.64$ fm. Blue and red bands signify the estimated uncertainties at NLO and N^{3}LO, respectively. The black solid line and diamonds denote the phase shift or mixing angle from the Nijmegen partial-wave analysis (NPWA) and lattice calculation at N^{3}LO, respectively.

only to consider the interactions that participate in a given channel, and our labeling of the operators makes clear which channels these are. We determine the LECs by reproducing the neutron-proton scattering phase shifts and mixing angles of the Nijmegen partial wave-analysis (NPWA) [23]. Since the NPWA provides only the statistical errors, and not the systematic errors, we use the procedure described in Ref. [16] to account for the systematic uncertainties. Specifically, we use

$$\Delta_X = \max\left(\Delta_X^{\rm NPWA}, \left|\delta_X^{\rm NijmI} - \delta_X^{\rm NPWA}\right|, \left|\delta_X^{\rm NijmII} - \delta_X^{\rm NPWA}\right|, \left|\delta_X^{\rm Reid93} - \delta_X^{\rm NPWA}\right|\right), \tag{74}$$

where δ_X^i are the phase shifts (mixing angles) in channel X based on different NPWA potentials, while $\Delta_X^{\rm NPWA}$ are the statistical errors of the phase shifts (mixing angles) of the NPWA.

For the coupled channel, $^3S_1$-$^3D_1$, we define the χ^2 as

$$\chi^2 = \sum_i \frac{\left(\delta_i^{\rm Latt} - \delta_i^{\rm NPWA}\right)^2}{\Delta_i^2} + \frac{\left(E_b^{\rm Latt} - E_b^{\rm Exp}\right)^2}{\Delta E_{\rm Exp}^2}, \tag{75}$$

with the deuteron binding energy $E_b^{\rm Exp} = 2.224\,575$ MeV and corresponding error $\Delta E_{\rm Exp} = 9 \times 10^{-6}$ MeV. For the other channels, we define χ^2 as

$$\chi^2 = \sum_i \frac{\left(\delta^{\rm Latt} - \delta_i^{\rm NPWA}\right)^2}{\Delta_i^2}. \tag{76}$$

In our fits we choose energy ranges that are appropriate for the chiral order and lattice spacing used. Specifically, for the coarser lattice spacings, $a = 1.97$ and 1.64 fm, we take the energy range $E_{\rm lab} \leqslant 50$ MeV for the LO, NLO/N^{2}LO, and N^{3}LO fits. In those cases we use five points, $E_{\rm lab} = 1$, 5, 10, 25, and 50 MeV, to compute the corresponding χ^2. For the fits with the smaller lattice spacings, $a = 1.32$ and 0.99 fm, we take the energy range $E_{\rm lab} \leqslant 50$ MeV for the LO, NLO, and N^{2}LO fits and $E_{\rm lab} \leqslant 100$ MeV for the N^{3}LO fits. Thus we determine the χ^2 for the N^{3}LO fits using six points, $E_{\rm lab} = 1$, 5, 10, 25, 50, and 100 MeV. The LECs determined by the N^{3}LO fits are listed in Table I for each of the lattice spacings.

In Fig. 2 we show the phase shifts and mixing angles versus the relative momenta calculated using the coarsest lattice spacings, $a = 1.97$ fm. We plot the results for relative momenta up to $p_{\rm rel} = 200$ MeV. The error bars we quote in this plot and in the following plots indicate uncertainties from the fitting procedure only. A more comprehensive analysis

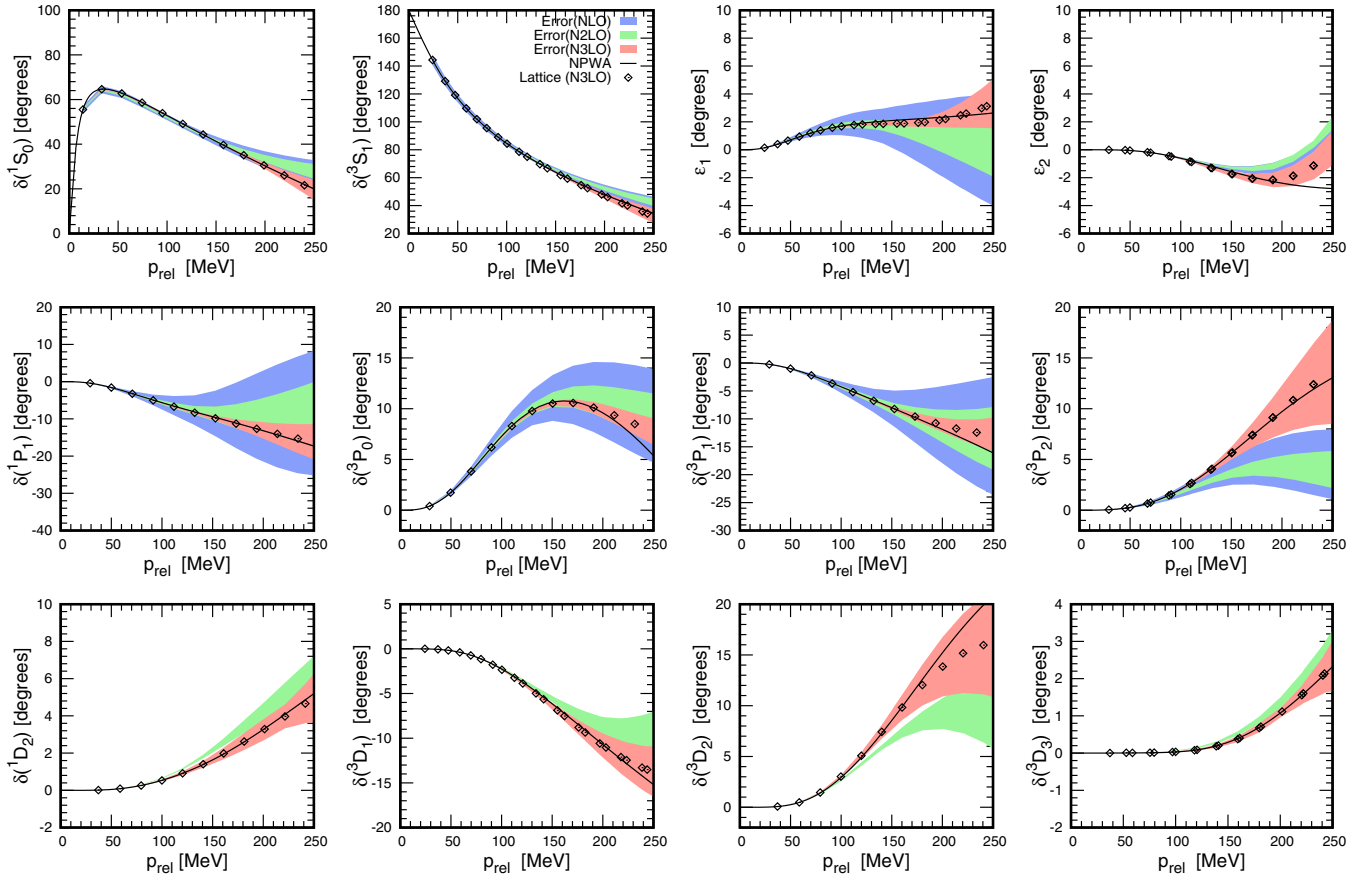

FIG. 11. Theoretical error bands for neutron-proton scattering phase shifts and mixing angles versus relative momenta for $a = 1.32$ fm with the full NN interaction. Blue, green, and red bands signify the estimated uncertainties at NLO, N^{2}LO, and N^{3}LO, respectively. The black solid line and diamonds denote the phase shift or mixing angle from the Nijmegen partial-wave analysis (NPWA) and lattice calculation at N^{3}LO, respectively.

that includes systematic errors due to the truncated chiral EFT expansion is presented later in our discussion. From the results, it is clear that with the new lattice operators the N^{3}LO calculations reproduce the NPWA phase shifts and mixing angles for most of the S, P, and D waves with a good accuracy for relative momenta less than 200 MeV. One can also see clearly that the agreement improves with chiral order. Unfortunately, the mixing angle ϵ_2 bends up for the relative momenta $p_{\rm rel}$ at around 150 MeV, which indicates that higher-order corrections, e.g., N4LO terms, or smaller lattice spacings would be needed to get the proper behavior for ϵ_2 at higher momenta.

In Fig. 3 we show the neutron-proton scattering phase shifts and mixing angles versus the relative momenta calculated using lattice spacing $a = 1.64$ fm. The results are very similar to those at $a = 1.97$ fm, but the mixing angle ϵ_2 stays accurate up to higher momenta compared with that at $a = 1.97$ fm. The smaller errors for the channels $^3P_2$ and ϵ_2 indicate that the results at $a = 1.64$ fm have smaller lattice artifacts than those at $a = 1.97$ fm, as one might expect.

For calculations involving the two smaller lattice spacings, $a = 1.32$ and 0.99 fm, we use the full NN interactions up to chiral order $O(Q^4)$ or N^{3}LO. The results are presented in Figs. 4 and 5, respectively. We plot the results for relative momenta up to $p_{\rm rel} = 250$ MeV. Compared to the results using the larger lattice spacings, one can see clear improvement. Again, good convergence is observed with increasing chiral order. With the full NN interactions up to order $O(Q^4)$, the calculation using $a = 0.99$ fm can describe the S, P, and D waves with a good accuracy over the whole momentum range, $0 < p_{\rm rel} < 250$ MeV.

To study the importance of the long-range part of the TPEP in the calculations, we also redo the same fits without the TPEP for $a = 1.32$ fm and $a = 0.99$ fm. Our results are shown in Figs. 6 and 7. For the calculations using $a = 1.32$ fm and $a = 0.99$ fm, the phase shifts and mixing angles without the TPEP are very similar to those with the TPEP, though the LECs are quite different. This indicates that the TPEP can be emulated by a retuning of the LECs. At the rather low scattering energies we probe, we do not see a clear improvement due to the TPEP from the phase shifts and mixing angles. However, we do expect that this will change at higher scattering energies.

IX. PROPERTIES OF THE DEUTERON

In this section, we calculate the properties of the deuteron using the radial deuteron wave function obtained in the

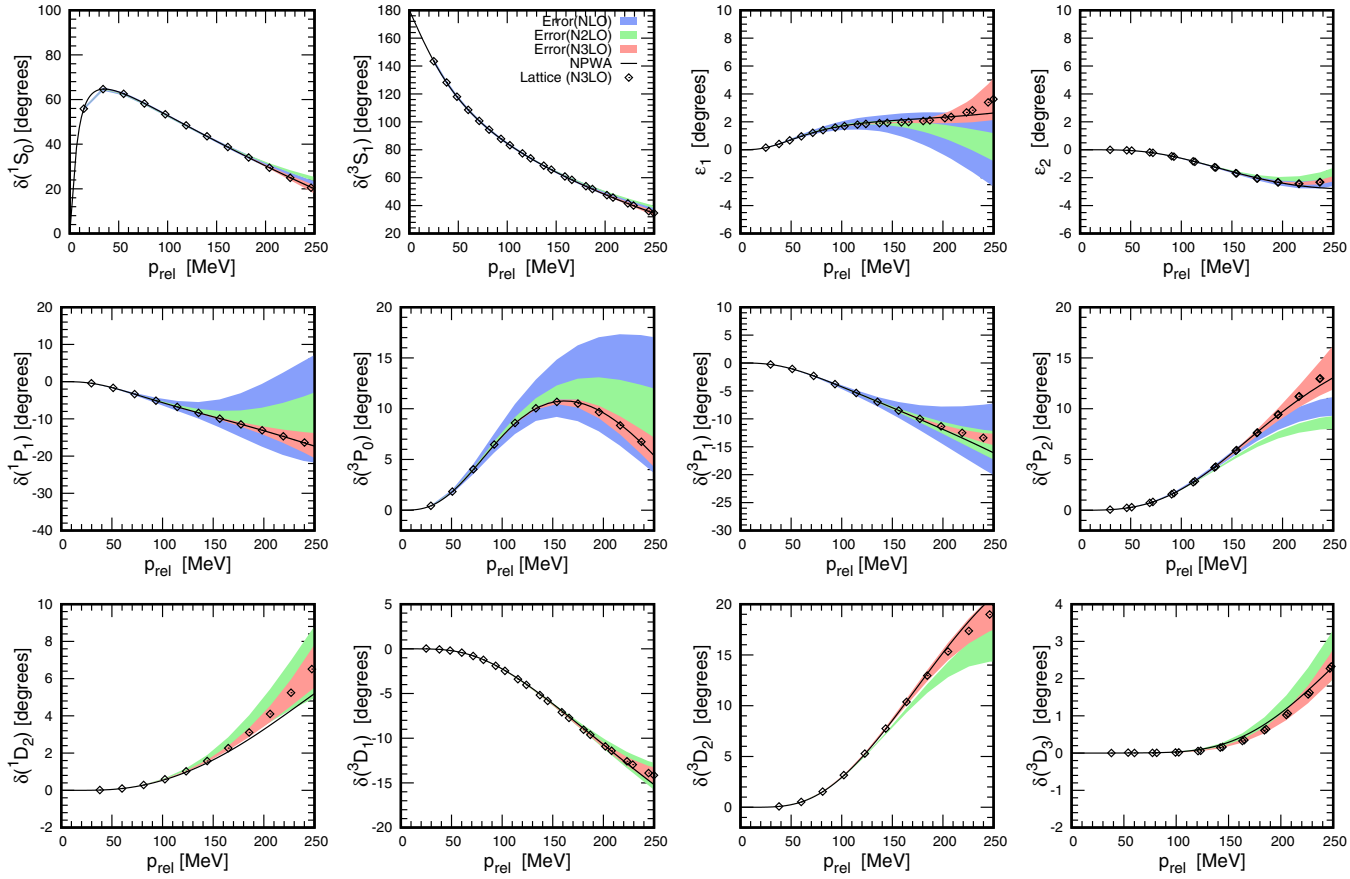

FIG. 12. Theoretical error bands for neutron-proton scattering phase shifts and mixing angles versus relative momenta for $a = 0.99$ fm with the full NN interaction. Blue, green, and red bands signify the estimated uncertainties at NLO, N^{2}LO, and N^{3}LO, respectively. The black solid line and diamonds denote the phase shift or mixing angle from the Nijmegen partial-wave analysis (NPWA) and lattice calculation at N^{3}LO, respectively.

calculations with $a = 0.99$ fm and the full NN interactions up to order Q^4 or N^{3}LO. At distance r beyond the range of the interaction, the radial wave function for the deuteron in the $^3S_1$ channel behaves as

$$u(r) = A_S e^{-\gamma r}, \tag{77}$$

where A_S is the S-wave asymptotic normalization coefficient. Here $\gamma = \sqrt{m|E_d|}$, with E_d denoting the deuteron binding energy. In the $^3D_1$ channel, the radial wave function behaves as

$$w(r) = \eta A_S \left[1 + \frac{3}{\gamma r} + \frac{3}{(\gamma r)^2}\right] e^{-\gamma r}. \tag{78}$$

In Fig. 8, we show the radial wave functions of the deuteron calculated using $a = 0.99$ fm with the full NN interaction up to chiral order $O(Q^4)$. The left panel shows the S-wave radial wave function while the right panel is for the D-wave radial wave function. In calculating the asymptotic normalization factors, we take the range $8 < r < 14$ fm. From the plots, one can see clearly that when the neutron and proton are well separated the S and D waves behave as the asymptotic forms in Eqs. (77) and (78), respectively. The numerical values for A_S and η are listed in Table II.

Using the radial wave functions, we can compute the root-mean-square radius of the deuteron,

$$r_d = \frac{1}{2}\left[\sum \delta r r^2 [u^2(r) + w^2(r)]\right]^{1/2}, \tag{79}$$

where δr is the small separation between the radial bins we are using for the radial deuteron wave function, and the summation is over all the radial bins. In the same manner, we can also compute the quadrupole moment of the deuteron,

$$Q_d = \frac{1}{20} \sum \delta r r^2 w(r)[\sqrt{8}u(r) - w(r)]. \tag{80}$$

In addition to the deuteron properties, we can also compute the S-wave effective range parameters at very low energies. The effective range expansion has the form

$$p \cot(\delta) = -\frac{1}{a} + \frac{1}{2} r p^2 + O(p^4), \tag{81}$$

where p is the relative momenta between the neutron and the proton, while a and r are the scattering length and effective range, respectively. Using these formula, we can extract the scattering length and effective range for $^3S_1$ and $^1S_0$.

In Table II, we present the properties of the deuteron and S-wave parameters obtained using the $a = 0.99$ fm and the

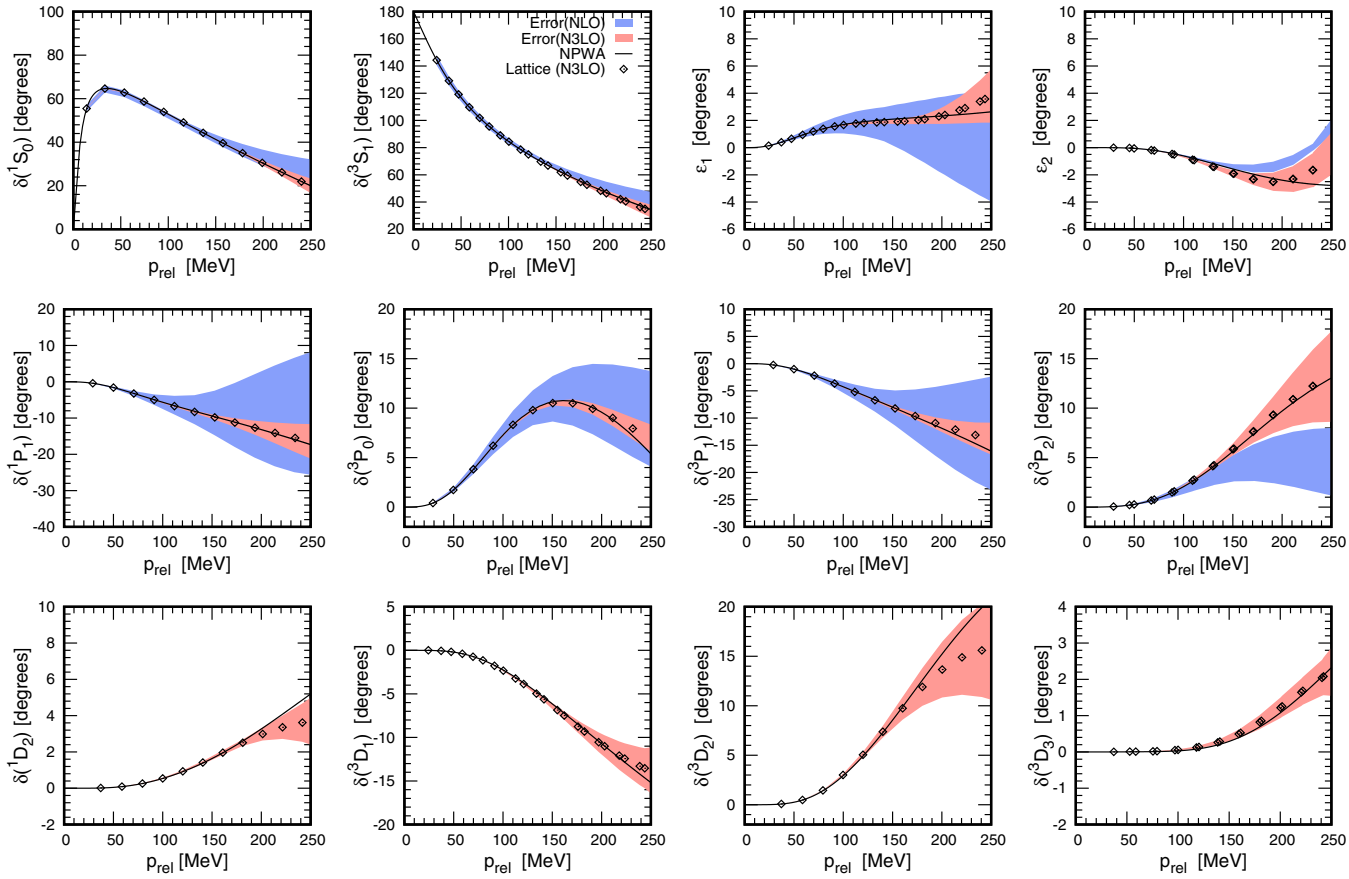

FIG. 13. Theoretical error bands for neutron-proton scattering phase shifts and mixing angles versus relative momenta for $a = 1.32$ fm without the TPEP. Blue and red bands signify the estimated uncertainties at NLO and N^{3}LO, respectively. The black solid line and diamonds denote the phase shift or mixing angle from the Nijmegen partial-wave analysis (NPWA) and lattice calculation at N^{3}LO, respectively.

full NN interactions up to order Q^4. In order to provide some insight into the nature of the lattice wave functions, we also list the computed D-wave probabilities of the deuteron, P_D. We note, however, that P_D is strongly dependent on short-distance physics and the scale at which it is regulated [30].

From the results in Table II, it is clear that the deuteron properties can be reproduced accurately at lattice spacing $a = 0.99$ fm. There are, however, still some small systematic discrepancies that suggest additional corrections are needed. While these could be due to corrections beyond N^{3}LO in the lattice Hamiltonian, they could also be due to missing corrections to the observables themselves such as the r^2 operator. Such corrections are needed to cancel ambiguities on how the operators are defined on a discrete lattice. For example, the nucleons could be regarded as exactly localized as delta functions at the lattice sites or they could be viewed as having some other distribution with a width comparable to the lattice spacing. While numerically small, these corrections to the operator observables are required for a full accounting of all lattice and regularization artifacts. See, for example, Ref. [31]. This is an interesting but extensive subject that requires further investigation in future studies.

X. THEORETICAL UNCERTAINTIES

It is necessary also to address the convergence of the effective field theory expansion on the lattice and their associated systematic errors. These important topics have generated much recent interest [16,32–34]. We follow the prescription in Refs. [16,32], where the theoretical uncertainty for some observable $X(p)$ at order N^{m}LO and momentum p is given by

$$\begin{aligned}\Delta X^{\mathrm{N}^m\mathrm{LO}}(p) = \max(&Q^{m+2}|X^{\mathrm{LO}}(p)|, Q^m|X^{\mathrm{LO}}(p) \\ &- X^{\mathrm{NLO}}(p)|, \ldots, Q^1|X^{\mathrm{N}^{m-1}\mathrm{LO}}(p) \\ &- X^{\mathrm{N}^m\mathrm{LO}}(p)|).\end{aligned} \tag{82}$$

Here Q is the estimated expansion parameter controlling the rate of convergence,

$$Q = \max(p/\Lambda_b, M_\pi/\Lambda_b), \tag{83}$$

and Λ_b the breakdown momentum scale. On the lattice, cubic symmetry replaces the rotational symmetry of the continuum, and the $(2L+1)$-dimensional irreducible representation of

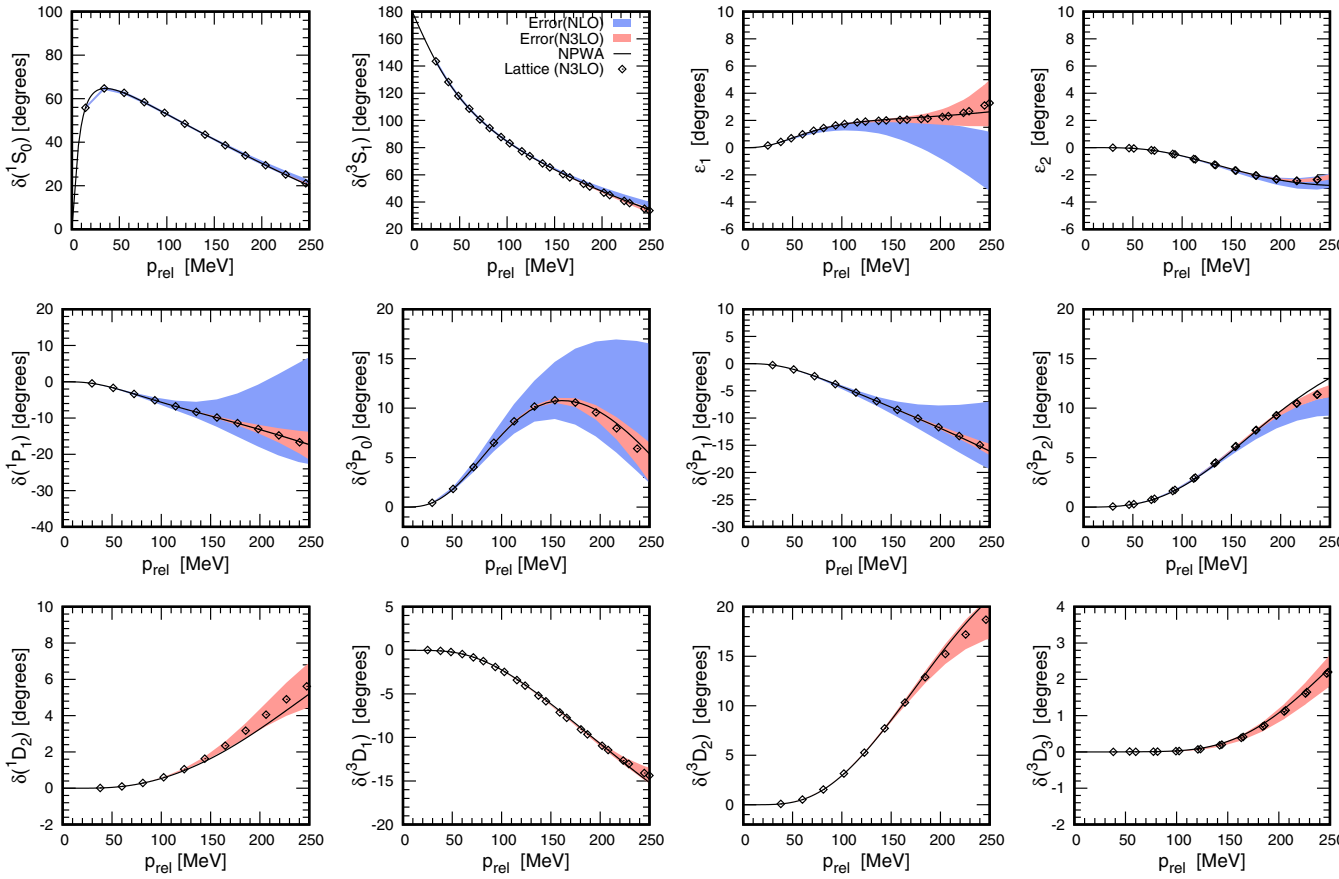

FIG. 14. Theoretical error bands for neutron-proton scattering phase shifts and mixing angles versus relative momenta for $a = 0.99$ fm without the TPEP. Blue and red bands signify the estimated uncertainties at NLO and N^{3}LO, respectively. The black solid line and diamonds denote the phase shift or mixing angle from the Nijmegen partial-wave analysis (NPWA) and lattice calculation at N^{3}LO, respectively.

SO(3) decomposes into irreducible representations of the rotational octahedral group O. For example, $L = 0$ corresponds to the A_1 of O, and $L = 1$ corresponds to the T_1 of O. However, $L = 2$ splits into the E and T_2 representations of O, and similar splittings occur in all of the larger L representations. As a result the breaking of rotational symmetry for $L \geqslant 2$ is numerically larger than that for $L < 2$. This leads to a lower momentum breakdown scale for D waves and above compared to S and P waves. To account for this in our calculations, we take Λ_b to be the lattice momentum cutoff $\Lambda_{\rm latt} = \pi/a$ for the lower partial waves, and we take $\Lambda_b = (2/3)\Lambda_{\rm latt}$ for ϵ_2, D waves, and higher partial waves.

We will study the dependence of the lattice breakdown scale on L and J in more detail in future work. The theoretical error bands for the neutron-proton scattering phase shifts and mixing angles versus the relative momenta for $a = 1.97$, 1.64, 1.32, and 0.99 fm are shown in Figs. 9–12, in which we see a systematic decrease in the uncertainties for the S- and D-wave phase shifts with decreasing lattice spacing. The unexpectedly small NLO uncertainties for the $^3P_0$ phase shifts at a coarse lattice spacing are caused by the rather good but accidental accuracy of the $^3P_0$ phase shifts at LO. We also show the estimated theoretical uncertainties for the neutron-proton scattering phase shifts and mixing angles for $a = 1.32$ and 0.99 fm without the long-range TPEP in Figs. 13 and 14. With only a few exceptions, the error bands for each order generally overlap with each other and cover the empirical phase shifts. This is a promising sign of convergence of the chiral effective field theory expansion on the lattice.

XI. SUMMARY AND OUTLOOK

We have proposed a new lattice formulation of the chiral NN force which is easily decomposed into partial waves. The new lattice operators work as projection operators, which only survive in particular channels. This advantage greatly simplifies the fitting procedure. Instead of fitting the phase shifts and mixing angles for all the channels simultaneously, only one uncoupled channel or two coupled channels are needed to be computed for each calculation.

To study the dependence on the lattice spacing, we have computed neutron-proton phase shifts and mixing angles using four lattice spacings, $a = 1.97$, 1.64, 1.32, and 0.99 fm. For two coarser lattice spacings, $a = 1.97$ or 1.64 fm, we did not explicitly include the TPEP, whereas for those using $a = 1.32$ or 0.99 fm, we did. Our numerical results indicate a good convergence with respect to chiral order. One also observes an obvious improvement when the lattice spacing is decreased.

Comparing the results obtained with and without the TPEP at lattice spacings of $a = 1.32$ and 0.99 fm, we did not find significant differences. This may, however, be a consequence of the rather low scattering energies we probe, and we expect that differences would appear at higher scattering energies.

We have also studied the properties of the deuteron wave function and the S-wave effective range parameters obtained with the full NN interaction at lattice spacing $a = 0.99$ fm. The numerical values are very close to the empirical values, which indicates that the current version of NN interactions is quite accurate and a very significant improvement over previous lattice studies. Some small discrepancies remain, but these may well be fixed in studies that reach a higher order in the chiral effective field theory expansion.

In summary, the new lattice interactions are far more efficient and accurate in reproducing physical data than previous lattice interactions. We have begun studying the properties of light- and medium-mass nuclei using these interactions, and the results are promising. These interactions were specifically designed to facilitate very efficient Monte Carlo simulations of few- and many-body systems using auxiliary fields. The results of these studies using these new interactions will be reported in several future publications.

ACKNOWLEDGMENTS

We acknowledge partial financial support from the Deutsche Forschungsgemeinschaft (TRR110, Symmetries and the Emergence of Structure in QCD), the BMBF (Grant No. 05P15PCFN1), the US Department of Energy (DE-SC0018638), and the Scientific and Technological Research Council of Turkey (TUBITAK Project No. 116F400). Further support was provided by the Chinese Academy of Sciences (CAS) President's International Fellowship Initiative (PIFI; Grant No. 2018DM0034) and by VolkswagenStiftung (Grant No. 93562). The computational resources were provided by the Jülich Supercomputing Centre at Forschungszentrum Jülich, Oak Ridge Leadership Computing Facility, RWTH Aachen, North Carolina State University, and Michigan State University.

[1] E. Epelbaum, H.-W. Hammer, and U.-G. Meißner, Rev. Mod. Phys. **81**, 1773 (2009).
[2] E. Epelbaum, H. Krebs, D. Lee, and U.-G. Meißner, Phys. Rev. Lett. **106**, 192501 (2011).
[3] E. Epelbaum, H. Krebs, T. Lähde, D. Lee, and U.-G. Meißner, Phys. Rev. Lett. **109**, 252501 (2012).
[4] E. Epelbaum, H. Krebs, T. A. Lähde, D. Lee, U.-G. Meißner, and G. Rupak, Phys. Rev. Lett. **112**, 102501 (2014).
[5] S. Elhatisari, D. Lee, G. Rupak, E. Epelbaum, H. Krebs, T. A. Lähde, T. Luu, and U.-G. Meißner, Nature **528**, 111 (2015).
[6] S. Elhatisari, N. Li, A. Rokash, J. M. Alarcon, D. Du, N. Klein, B. N. Lu, U.-G. Meißner, E. Epelbaum, H. Krebs, T. A. Lahde, D. Lee, and G. Rupak, Phys. Rev. Lett. **117**, 132501 (2016).
[7] S. Elhatisari, E. Epelbaum, H. Krebs, T. A. Lähde, D. Lee, N. Li, B.-n. Lu, U.-G. Meißner, and G. Rupak, Phys. Rev. Lett. **119**, 222505 (2017).
[8] J. M. Alarcón, D. Du, N. Klein, T. A. Lähde, D. Lee, N. Li, B.-N. Lu, T. Luu, and U.-G. Meißner, Eur. Phys. J. A **53**, 83 (2017).
[9] N. Klein, S. Elhatisari, T. A. Lähde, D. Lee, and U.-G. Meißner, Eur. Phys. J. A **54**, 121 (2018).
[10] D. Lee, Prog. Part. Nucl. Phys. **63**, 117 (2009).
[11] E. Wigner, Phys. Rev. **51**, 106 (1937).
[12] P. Reinert, H. Krebs, and E. Epelbaum, Eur. Phys. J. A **54**, 86 (2018).
[13] B. Borasoy, E. Epelbaum, H. Krebs, D. Lee, and U.-G. Meißner, Eur. Phys. J. A **35**, 343 (2008).
[14] S. Weinberg, Phys. Lett. B **251**, 288 (1990).
[15] N. Kaiser, Phys. Rev. C **64**, 057001 (2001).
[16] E. Epelbaum, H. Krebs, and U.-G. Meißner, Eur. Phys. J. A **51**, 53 (2015).
[17] D. R. Entem, N. Kaiser, R. Machleidt, and Y. Nosyk, Phys. Rev. C **91**, 014002 (2015).
[18] E. Epelbaum, W. Glöckle, and U.-G. Meißner, Nucl. Phys. A **747**, 362 (2005).
[19] D. Lee and R. Thomson, Phys. Rev. C **75**, 064003 (2007).
[20] B.-N. Lu, T. A. Lähde, D. Lee, and U.-G. Meißner, Phys. Lett. B **760**, 309 (2016).
[21] S. Elhatisari, D. Lee, U.-G. Meißner, and G. Rupak, Eur. Phys. J. A **52**, 174 (2016).
[22] H. P. Stapp, T. J. Ypsilantis, and N. Metropolis, Phys. Rev. **105**, 302 (1957).
[23] V. G. J. Stoks, R. A. M. Klomp, M. C. M. Rentmeester, and J. J. de Swart, Phys. Rev. C **48**, 792 (1993).
[24] C. Van Der Leun and C. Alderliesten, Nucl. Phys. A **380**, 261 (1982).
[25] T. E. O. Ericson and M. Rosa-Clot, Nucl. Phys. A **405**, 497 (1983).
[26] N. L. Rodning and L. D. Knutson, Phys. Rev. C **41**, 898 (1990).
[27] D. M. Bishop and L. M. Cheung, Phys. Rev. A **20**, 381 (1979).
[28] A. Huber, T. Udem, B. Gross, J. Reichert, M. Kourogi, K. Pachucki, M. Weitz, and T. W. Hansch, Phys. Rev. Lett. **80**, 468 (1998).
[29] O. Dumbrajs, R. Koch, H. Pilkuhn, G. C. Oades, H. Behrens, J. J. De Swart, and P. Kroll, Nucl. Phys. B **216**, 277 (1983).
[30] J. L. Friar, Phys. Rev. C **20**, 325 (1979).
[31] N. Klein, D. Lee, and U.-G. Meißner, arXiv:1807.04234 [hep-lat] (2018).
[32] E. Epelbaum, H. Krebs, and U.-G. Meißner, Phys. Rev. Lett. **115**, 122301 (2015).
[33] R. J. Furnstahl, D. R. Phillips, and S. Wesolowski, J. Phys. G **42**, 034028 (2015).
[34] R. J. Furnstahl, N. Klco, D. R. Phillips, and S. Wesolowski, Phys. Rev. C **92**, 024005 (2015).